

Estimation and Statistical Inference for Generalized Multilayer Latent Space Model

Zhaozhe Liu[†], Gongjun Xu[‡] and Haoran Zhang[†]

[†]Department of Statistics and Data Science
Southern University of Science and Technology

[‡] Department of Statistics
University of Michigan

Abstract

Multilayer networks have become increasingly ubiquitous across diverse scientific fields, ranging from social sciences and biology to economics and international relations. Despite their broad applications, the inferential theory for multilayer networks remains underdeveloped. In this paper, we propose a flexible latent space model for multilayer directed networks with various edge types, where each node is assigned with two latent positions capturing sending and receiving behaviors, and each layer has a connection matrix governing the layer-specific structure. Through nonlinear link functions, the proposed model represents the structure of a multilayer network as a tensor, which admits a Tucker low-rank decomposition. This formulation poses significant challenges on the estimation and statistical inference for the latent positions and connection matrices, where existing techniques are inapplicable. To tackle this issue, a novel unfolding and fusion method is developed to facilitate estimation. We establish both consistency and asymptotic normality for the estimated latent positions and connection matrices, which paves the way for statistical inference tasks in multilayer network applications, such as constructing confidence regions for the latent positions and testing whether two network layers share the same structure. We validate the proposed method through extensive simulation studies and demonstrate its practical utility on real-world data.

KEY WORDS: latent space model, network embedding, Tucker tensor decomposition, asymptotic distribution, change point detection

1 Introduction

Multilayer networks serve as a powerful representation for relational data, in which nodes correspond to entities and edges across different layers capture multiple types of relationships among them. Such networks have become increasingly prevalent in a variety of real-world applications, including biological networks (Liu et al., 2020; Núñez-Carpintero et al., 2024), international trade networks (A. Alves et al., 2018; Ren et al., 2020; Jing et al., 2021), and social networks (Baggio et al., 2016; Dickison et al., 2016).

Over the last decade, many models and methods have been developed to facilitate analysis for multilayer networks. For example, community detection for multilayer networks has been extensively studied, based on the multilayer stochastic block model and its variants (Paul and Chen, 2016; Barbillon et al., 2017; Wilson et al., 2017; Yuan and Qu, 2021; Jing et al., 2021). Various methods have been developed for community detection, including the spectral methods (Bhattacharyya and Chatterjee, 2017; Xie, 2024), maximum likelihood estimates (Han et al., 2015; Paul and Chen, 2016; Yuan and Qu, 2021), least square estimates (Lei et al., 2020), and tensor decomposition (Jing et al., 2021). Besides the multilayer stochastic block model, multilayer latent space models (Gollini and Murphy, 2016; Salter-Townshend and McCormick, 2017; D’Angelo et al., 2019) are more flexible models for multilayer networks, which originate from the latent space model for a single network (Hoff et al., 2002). The common idea behind different multilayer latent space modeling is that, besides node-wise latent positions, there are additional layer-wise structure parameters, which correspond either to degree heterogeneity across layers (Gollini and Murphy, 2016; He et al., 2025) or to layer structures, such as layer-wise scalars, latent positions, or connection matrices (D’Angelo et al., 2019; Zhang et al., 2020b; MacDonald et al., 2022; Zhang and Wang, 2025). Average consistency results of the maximum likelihood estimators for latent positions have been established (Zhang et al., 2020b; MacDonald et al., 2022; Zhang and

Wang, 2025). Recently, based on a semiparametric dynamic latent space model, He et al. (2025) established the uniform convergence rate for the estimated latent positions by solving an efficient score estimation equation.

Although multilayer networks are frequently encountered in practice and theoretical results have been established for various methods, statistical inference for multilayer network models is still at its early stage, which is important in quantifying the estimation uncertainty for latent positions and layer-specific structures, as well as downstream tasks such as link prediction and network testing. Recently, a few works have established the inferential theory under the multilayer stochastic block model. In particular, Arroyo et al. (2021) and Xie (2024) derived the asymptotic distributions for the eigenvectors and the layer-specific connection matrices under the common subspace independent edge (COSIE) random graph model, and Su et al. (2026) obtained the asymptotic distributions for the connection matrices under the multilayer stochastic block model. However, both models assume that the binary edges follow linear models, which may not be the most suitable choice for more general settings where discrete edges are modeled through nonlinear link functions, as commonly encountered in many applications.

To see the challenge of the statistical inference for multilayer network models with nonlinear link functions, we note that the distribution of a multilayer network is determined by an underlying order-3 tensor with two node-wise dimensions and one layer-wise dimension, which, through nonlinear link functions, admits a low-rank Tucker decomposition under the multilayer latent space model discussed in Section 2. Then, the latent positions correspond to the loading matrices while the layer-specific connection matrices form the core tensor in the Tucker decomposition. In the existing literature, there have been only results on the estimation and uncertainty quantification for the loading matrices in a Tucker tensor decomposition (Xia et al., 2022; Agterberg and Zhang, 2024) under linear tensor models. However, the asymptotic distribution for the core tensor estimator remains largely unknown, and the

presence of nonlinear link functions introduces additional layers of technical difficulty.

The contributions of this paper are summarized as follows.

1. We propose a new multilayer latent space model for multilayer directed networks, which allows different types of edges, including binary, continuous and counting types, through general edge-specific link functions. The model assigns two latent positions for each node to capture its sending and receiving behaviors. The probability distribution for a directed edge between two nodes in a specific layer depends on the inner product of their latent positions through a layer-specific connection matrix, which determines how nodes interact with each other in this layer. Furthermore, each node also has two degree parameters in each layer, which account for degree heterogeneity in the multilayer network. Our framework is flexible and general, encompassing many existing multilayer network models as special cases (see Remark 2).
2. A novel *Unfolding and Fusion* method is proposed for estimating the node-specific latent positions and layer-specific connection matrices. Specifically, we first aggregate all network layers to form a tensor. To estimate the latent positions controlling the node sending behaviors, we unfold the aggregated tensor in the first direction and estimate the underlying low-rank matrix through a maximum likelihood estimate. Then, the latent position estimators are obtained from the left singular vectors of the estimated low-rank matrix, after partialing out the effect of degree parameters through a two-sided centering operator. Similarly, the latent positions for receiving behaviors are estimated based on the unfolding in the second dimension. For the layer-specific connection matrices, we adopt a fusion strategy. In particular, the estimator is formed by combining the right singular vectors of the estimated low-rank matrix from unfolding in the first direction, and the left singular vectors of the estimated low-rank matrix from unfolding in the second direction. The proposed *Unfolding and Fusion*

method only involves two optimizations regarding low rank matrices, which enables us to exploit the rich results in the literature of low-rank matrix estimation and factor analysis. Moreover, it circumvents direct large-scale tensor optimization which is highly non-convex and computationally intensive.

3. We further establish asymptotic distributions for the estimated latent positions and connection matrices. For latent positions, to tackle the identifiability issue, we derive their asymptotic normality by carefully analyzing the Hessian matrix of the Lagrangian regularized log likelihood functions for the unfolding parameter matrices. To derive the asymptotic normality for estimated connection matrices, thanks to the fusion structure, we combine the first order expansions for the estimated left and right singular matrices obtained from the optimizations based on the unfolding along two dimensions. The established results not only provide valid uncertainty quantification for the proposed estimators but also facilitate downstream inference tasks in multilayer network applications, such as testing whether two network layers share the same structure. To the best of our knowledge, this is one of the first inferential theories developed for nonlinear multilayer network models.

The remainder of the paper is organized as follows. Section 1.1 introduces the notation and preliminary results on matrix and tensor operations. Section 2 describes the proposed model. Estimation procedures are developed in Section 2.3, and the corresponding theoretical results are presented in Section 3. Section 4 reports numerical results for both synthetic and real data. Section 5 summarizes the main results and lists some future directions. Technical proofs and more numerical results are included in the supplementary material.

1.1 Notations and preliminaries.

We introduce some notations and definitions here, which are necessary throughout this paper and the supplement. For any integer K , let $[K] = \{1, \dots, K\}$. We use $\text{vec}(\cdot)$ to denote the column-wise vectorization of matrices, and \otimes for the Kronecker product. The ψ_1 -Orlicz norm of a random variable \mathbf{X} , where $\psi_1(x) = \exp(x) - 1$, is defined as $\|\mathbf{X}\|_{\psi_1} := \inf\{t > 0 : \mathbb{E}[\exp(|\mathbf{X}|/t)] \leq 2\}$. Note that \mathbf{X} is sub-exponential if $\|\mathbf{X}\|_{\psi_1} < \infty$.

For any $mr \times 1$ vector \mathbf{v} consisting of m blocks of $r \times 1$ small vectors, $[\mathbf{v}]_i = \mathbf{v}_{(i-1)r+1:ir,1}$ for any $1 \leq i \leq m$, where $[\mathbf{v}]_i$ represents the i -th ($r \times 1$) sub-block of \mathbf{v} . Moreover, for any $1 \leq j \leq r$, $[[\mathbf{v}]_i]_j = \mathbf{v}_{(i-1)r+j,1}$. In a word, $[[\mathbf{v}]_i]_j$ denotes the j -th element of the i -th ($r \times 1$) sub-block. For any matrix \mathbf{A} , let $\mathbf{A}_{i,j}$ be its (i, j) -th entry. We also denote $\mathbf{A}_{i,:}$ as its i -th row and $\mathbf{A}_{:,j}$ as the j -th column. The $\ell_{2,\infty}$ -norm of matrix \mathbf{A} is defined as $\|\mathbf{A}\|_{2,\infty} = \max_i \|\mathbf{A}_{i,:}\|_2$.

For any tensor $\mathcal{X} \in \mathbb{R}^{d_1 \times d_2 \times d_3}$, let $\mathcal{X}_{i,j,t}$ denote its (i, j, t) -th entry. Let $\mathcal{M}_m(\cdot)$ denote the mode- m unfolding of a 3-dimensional tensor into a matrix. Specifically, $\mathcal{M}_1(\mathcal{X}) \in \mathbb{R}^{d_1 \times (d_2 d_3)}$ with $\mathcal{X}_{i_1, i_2, i_3} = [\mathcal{M}_1(\mathcal{X})]_{i_1, i_2 + d_2(i_3 - 1)}$, and $\mathcal{M}_2(\mathcal{X}) \in \mathbb{R}^{d_2 \times (d_1 d_3)}$ with $\mathcal{X}_{i_1, i_2, i_3} = [\mathcal{M}_2(\mathcal{X})]_{i_2, i_1 + d_1(i_3 - 1)}$. For $n, T \in \mathbb{N}^+$, let $\mathcal{A} \in \mathbb{R}^{1 \times n \times T}$ be a tensor with $\mathcal{M}_2(\mathcal{A}) = \boldsymbol{\alpha} \in \mathbb{R}^{n \times T}$, and $\mathcal{B} \in \mathbb{R}^{n \times 1 \times T}$ with $\mathcal{M}_1(\mathcal{B}) = \boldsymbol{\beta} \in \mathbb{R}^{n \times T}$. Then, the following unfolding identities hold:

$$\begin{aligned}
\mathcal{M}_1(\mathcal{A} \times_1 \mathbf{1}_n) &= \mathcal{M}_1([\mathcal{A}; \mathbf{1}_n, \mathbf{I}_n, \mathbf{I}_T]) = \mathbf{1}_n \text{vec}(\boldsymbol{\alpha})^\top, \\
\mathcal{M}_2(\mathcal{A} \times_1 \mathbf{1}_n) &= \mathcal{M}_2([\mathcal{A}; \mathbf{1}_n, \mathbf{I}_n, \mathbf{I}_T]) = \boldsymbol{\alpha}(\mathbf{I}_T \otimes \mathbf{1}_n^\top), \\
\mathcal{M}_1(\mathcal{B} \times_2 \mathbf{1}_n) &= \mathcal{M}_1([\mathcal{B}; \mathbf{I}_n, \mathbf{1}_n, \mathbf{I}_T]) = \boldsymbol{\beta}(\mathbf{I}_T \otimes \mathbf{1}_n^\top), \\
\mathcal{M}_2(\mathcal{B} \times_2 \mathbf{1}_n) &= \mathcal{M}_2([\mathcal{B}; \mathbf{I}_n, \mathbf{1}_n, \mathbf{I}_T]) = \mathbf{1}_n \text{vec}(\boldsymbol{\beta})^\top.
\end{aligned} \tag{1}$$

2 Proposed Method

2.1 Generalized Multilayer Latent Space Model

Let \mathcal{G} denote a multilayer directed network comprising T network layers on n common nodes. For any $t \in [T]$, the t -th network layer can be represented via its adjacency matrix $(y_{ijt})_{n \times n}$, where y_{ijt} indicates the directed interaction from node i to node j on the t -th layer. We assume each y_{ijt} is generated from

$$y_{ijt} \sim g_{ijt}(\cdot \mid x_{ijt}), \quad \text{with } x_{ijt} = \boldsymbol{\theta}_i^\top \boldsymbol{\Lambda}_t \boldsymbol{\phi}_j + \beta_{it} + \alpha_{jt}, \quad (2)$$

where $g_{ijt}(\cdot \mid \cdot)$ is some known probability density/mass function, which is allowed to vary across different node pairs (i, j) and layers t . Here the directed interaction effect from node i to node j on the t -th layer is modeled through $\boldsymbol{\theta}_i^\top \boldsymbol{\Lambda}_t \boldsymbol{\phi}_j$, where $\boldsymbol{\theta}_i \in \mathbb{R}^{k_1}$ and $\boldsymbol{\phi}_j \in \mathbb{R}^{k_2}$ are respectively the latent positions capturing the sending and receiving behavior of nodes i and j , and $\boldsymbol{\Lambda}_t \in \mathbb{R}^{k_1 \times k_2}$ is a layer-specific connection matrix governing the interaction structure of the t -th layer. Further, β_{it} and α_{jt} are respectively the out-degree and in-degree heterogeneity parameters for nodes i and j on the t -th layer. We suppose all y_{ijt} are independent conditioning on $\{\boldsymbol{\theta}_i\}_{i=1}^n$, $\{\boldsymbol{\phi}_j\}_{j=1}^n$, $\{\alpha_{it}, \beta_{it}\}_{i \in [n], t \in [T]}$ and $\{\boldsymbol{\Lambda}_t\}_{t=1}^T$.

Remark 1. *The flexibility on the distribution functions g_{ijt} 's allows us to deal with networks with different kinds of edge types, including binary, count, and continuous data types. For such types of edges, the exponential family of distributions can be used for modeling (Rabe-Hesketh and Skrondal, 2004), whose density takes the form $g_{ijt}(y) = \exp\{(yx_{ijt} - b_{ijt}(x_{ijt}))/\phi_{ijt} - c_{ijt}(y, \phi_{ijt})\}$, where b_{ijt}, c_{ijt} are known functions and ϕ_{ijt} is the dispersion parameter. If y_{ijt} is continuous, we may assume g_{ijt} is a Gaussian density function, where ϕ_{ijt} is the variance, $b_{ijt}(x_{ijt}) = x_{ijt}^2/2$ and $c_{ijt}(y_{ijt}, \phi_{ijt}) = -y_{ijt}^2/(2\phi_{ijt}^2) - \frac{1}{2} \log(2\pi\phi_{ijt}^2)$. For binary $y_{ijt} \in \{0, 1\}$, we can assume it follows a logistic model with $\phi_{ijt} = 1$, $b_{ijt}(x_{ijt}) = \log(1 + e^{x_{ijt}})$*

and $c_{ijt}(y_{ijt}, \phi_{ijt}) = 0$. A Poisson model may be assumed if y_{ijt} is a count variable, where $\phi_{ijt} = 1$, $b_{ijt}(x_{ijt}) = e^{x_{ijt}}$, $c_{ijt}(y_{ijt}, \phi_{ijt}) = -\log(y_{ijt}!)$.

Remark 2. The model (2) includes many existing network models as special cases. For undirected networks, we set $k_1 = k_2$, $\boldsymbol{\theta}_i = \boldsymbol{\phi}_i$ and $\beta_{it} = \alpha_{it}$. If all y_{ijt} for $i \neq j$ are Bernoulli random variables with mean $1/(1 + e^{x_{ijt}})$, then (2) becomes the multilayer latent space model in Zhang et al. (2020b). If all y_{ijt} are Bernoulli random variables with mean x_{ijt} and $\beta_{it} = \alpha_{it} = 0$, then (2) reduces to the COSIE random graph model (Arroyo et al., 2021). If all y_{ijt} are Poisson random variables with mean $e^{x_{ijt}}$ and $\boldsymbol{\Lambda}_t = \mathbf{I}_k$, then (2) is equivalent to the Poisson-based latent space model in He et al. (2025). For directed networks, if all y_{ijt} are Poisson random variables with mean $e^{x_{ijt}}$ with $\beta_{it} = \alpha_{jt} \equiv \text{const}$ and $\text{vec}(\boldsymbol{\Lambda}_t) = \mathbf{M}\mathbf{w}_t$ for some $\mathbf{M} \in \mathbb{R}^{k_1 k_2 \times r}$ and $\mathbf{w}_t \in \mathbb{R}^r$, then (2) is the same as the dynamic network embedding model in Zhang and Wang (2025).

Let $\mathcal{X} = (x_{ijt})_{n \times n \times T}$, $\boldsymbol{\Theta} = (\boldsymbol{\theta}_1, \dots, \boldsymbol{\theta}_n)^\top$ and $\boldsymbol{\Phi} = (\boldsymbol{\phi}_1, \dots, \boldsymbol{\phi}_n)^\top$. For $t \in [T]$, define $\mathbf{X}_t = (x_{ijt})_{n \times n}$, $\boldsymbol{\alpha}_t = (\alpha_{1t}, \dots, \alpha_{nt})^\top$, $\boldsymbol{\beta}_t = (\beta_{1t}, \dots, \beta_{nt})^\top$. Further define $\boldsymbol{\alpha} = (\boldsymbol{\alpha}_1, \dots, \boldsymbol{\alpha}_T)$ and $\boldsymbol{\beta} = (\boldsymbol{\beta}_1, \dots, \boldsymbol{\beta}_T)$. Then,

$$\mathbf{X}_t = \boldsymbol{\Theta}\boldsymbol{\Lambda}_t\boldsymbol{\Phi}^\top + \mathbf{1}_n\boldsymbol{\alpha}_t^\top + \boldsymbol{\beta}_t\mathbf{1}_n^\top, \quad t \in [T]. \quad (3)$$

To facilitate estimation, it is helpful to represent \mathcal{X} in a tensor product form. To this end, define tensors $\mathcal{A} \in \mathbb{R}^{1 \times n \times T}$ and $\mathcal{B} \in \mathbb{R}^{n \times 1 \times T}$ such that $\mathcal{A}_{1, :, t} = \boldsymbol{\alpha}_t$ and $\mathcal{B}_{:, 1, t} = \boldsymbol{\beta}_t$. Further, define a tensor $\mathcal{S} \in \mathbb{R}^{k_1 \times k_2 \times T}$ such that $\mathcal{S}_{:, :, t} = \boldsymbol{\Lambda}_t$ for $t \in [T]$. Then, by (1) and (3),

$$\mathcal{X} = [\mathcal{S}; \boldsymbol{\Theta}, \boldsymbol{\Phi}, \mathbf{I}_T] + [\mathcal{A}; \mathbf{1}_n, \mathbf{I}_n, \mathbf{I}_T] + [\mathcal{B}; \mathbf{I}_n, \mathbf{1}_n, \mathbf{I}_T]. \quad (4)$$

To reduce model complexity, we adopt a factor modeling for both $\boldsymbol{\alpha} \in \mathbb{R}^{n \times T}$ and $\boldsymbol{\beta} \in \mathbb{R}^{n \times T}$, which is reasonable especially when both n, T are large (Bai and Li, 2012;

Fan et al., 2016; Chen et al., 2020). Specifically, there exist $\mathbf{U}_\alpha \in \mathbb{R}^{n \times k_\alpha}$, $\mathbf{U}_\beta \in \mathbb{R}^{n \times k_\beta}$, $\mathbf{V}_\alpha \in \mathbb{R}^{T \times k_\alpha}$, $\mathbf{V}_\beta \in \mathbb{R}^{T \times k_\beta}$ such that

$$\boldsymbol{\alpha} = \mathbf{U}_\alpha \mathbf{V}_\alpha^\top \quad \text{and} \quad \boldsymbol{\beta} = \mathbf{U}_\beta \mathbf{V}_\beta^\top. \quad (5)$$

According to (1) and (4), unfolding \mathcal{X} along the first mode yields

$$\begin{aligned} \mathcal{M}_1(\mathcal{X}) &= \boldsymbol{\Theta} \mathcal{M}_1(\mathcal{S}) (\mathbf{I}_T \otimes \boldsymbol{\Phi}^\top) + \boldsymbol{\beta} (\mathbf{I}_T \otimes \mathbf{1}_n^\top) + \mathbf{1}_n \text{vec}(\boldsymbol{\alpha})^\top \\ &= \begin{pmatrix} \boldsymbol{\Theta} & \mathbf{U}_\beta & \mathbf{1}_n \end{pmatrix} \begin{pmatrix} \mathcal{M}_1(\mathcal{S}) (\mathbf{I}_T \otimes \boldsymbol{\Phi}^\top) \\ \mathbf{V}_\beta^\top (\mathbf{I}_T \otimes \mathbf{1}_n^\top) \\ \text{vec}(\boldsymbol{\alpha})^\top \end{pmatrix} =: \mathbf{U}_1 \mathbf{V}_1^\top, \end{aligned} \quad (6)$$

with

$$\mathbf{U}_1 := \begin{pmatrix} \boldsymbol{\Theta} & \mathbf{U}_\beta & \mathbf{1}_n \end{pmatrix}, \quad \mathbf{V}_1 := \begin{pmatrix} (\mathbf{I}_T \otimes \boldsymbol{\Phi}) \mathcal{M}_1(\mathcal{S})^\top & (\mathbf{I}_T \otimes \mathbf{1}_n) \mathbf{V}_\beta & \text{vec}(\boldsymbol{\alpha}) \end{pmatrix}, \quad (7)$$

where $\mathbf{U}_1 \in \mathbb{R}^{n \times d_1}$ and $\mathbf{V}_1 \in \mathbb{R}^{(nT) \times d_1}$ with $d_1 := k_1 + k_\beta + 1$ constitute a low-rank factorization of $\mathcal{M}_1(\mathcal{X})$. Similarly, unfolding \mathcal{X} along the second mode gives

$$\begin{aligned} \mathcal{M}_2(\mathcal{X}) &= \boldsymbol{\Phi} \mathcal{M}_2(\mathcal{S}) (\mathbf{I}_T \otimes \boldsymbol{\Theta}^\top) + \boldsymbol{\alpha} (\mathbf{I}_T \otimes \mathbf{1}_n^\top) + \mathbf{1}_n \text{vec}(\boldsymbol{\beta})^\top \\ &= \begin{pmatrix} \boldsymbol{\Phi} & \mathbf{U}_\alpha & \mathbf{1}_n \end{pmatrix} \begin{pmatrix} \mathcal{M}_2(\mathcal{S}) (\mathbf{I}_T \otimes \boldsymbol{\Theta}^\top) \\ \mathbf{V}_\alpha^\top (\mathbf{I}_T \otimes \mathbf{1}_n^\top) \\ \text{vec}(\boldsymbol{\beta})^\top \end{pmatrix} =: \mathbf{U}_2 \mathbf{V}_2^\top, \end{aligned} \quad (8)$$

where $\mathbf{U}_2 \in \mathbb{R}^{n \times d_2}$ and $\mathbf{V}_2 \in \mathbb{R}^{nT \times d_2}$ with $d_2 := k_2 + k_\alpha + 1$ represent the corresponding

low-rank factors in $\mathcal{M}_2(\mathcal{X})$, with explicit forms:

$$\mathbf{U}_2 := \begin{pmatrix} \Phi & \mathbf{U}_\alpha & \mathbf{1}_n \end{pmatrix}, \quad \mathbf{V}_2 := \begin{pmatrix} (\mathbf{I}_T \otimes \Theta) \mathcal{M}_2(\mathcal{S})^\top & (\mathbf{I}_T \otimes \mathbf{1}_n) \mathbf{V}_\alpha & \text{vec}(\beta) \end{pmatrix}. \quad (9)$$

2.2 Identifiability

Note that there is an identifiability issue for the model parameters. Let Θ^* , Φ^* , \mathbf{U}_α^* , \mathbf{U}_β^* , \mathbf{V}_α^* , \mathbf{V}_β^* , \mathcal{S}^* and \mathcal{X}^* be the true parameter matrices and tensors from (4) and (5). Then, for any invertible matrices $\mathbf{F}_1 \in \mathbb{R}^{k_1 \times k_2}$ and $\mathbf{F}_2 \in \mathbb{R}^{k_2 \times k_2}$, we have

$$[\mathcal{S}^*; \Theta^*, \Phi^*, \mathbf{I}_T] = [\mathcal{S}^* \times_1 \mathbf{F}_1^{-1} \times_2 \mathbf{F}_2^{-1}; \Theta^* \mathbf{F}_1^\top, \Phi^* \mathbf{F}_2^\top, \mathbf{I}_T],$$

which makes it impossible to distinguish $(\mathcal{S}^*, \Theta^*, \Phi^*)$ and $(\mathcal{S}^* \times_1 \mathbf{F}_1^{-1} \times_2 \mathbf{F}_2^{-1}, \Theta^* \mathbf{F}_1^\top, \Phi^* \mathbf{F}_2^\top)$ without further conditions. We now establish the identifiability conditions for the parameters of interest, specifically the Θ^* , Φ^* and \mathcal{S}^* . Let us first consider Θ^* and Φ^* . Define the centering matrix $\mathbf{J}_n = \mathbf{I}_n - n^{-1} \mathbf{1}_n \mathbf{1}_n^\top$ and the block-wise centering matrix $\mathbf{J}_{n,T} = \mathbf{I}_T \otimes \mathbf{J}_n$. We start by noting that, from (7) and (9),

$$\mathbf{J}_n \mathcal{M}_1(\mathcal{X}^*) \mathbf{J}_{n,T}^\top = \Theta^* \mathcal{M}_1(\mathcal{S}^*) (\mathbf{I}_T \otimes \Phi^{*\top}), \quad \mathbf{J}_n \mathcal{M}_2(\mathcal{X}^*) \mathbf{J}_{n,T}^\top = \Phi^* \mathcal{M}_2(\mathcal{S}^*) (\mathbf{I}_T \otimes \Theta^{*\top}), \quad (10)$$

which implies that Θ^* and Φ^* could be identified from the column spaces of $\mathbf{J}_n \mathcal{M}_1(\mathcal{X}^*) \mathbf{J}_{n,T}^\top$ and $\mathbf{J}_n \mathcal{M}_2(\mathcal{X}^*) \mathbf{J}_{n,T}^\top$, respectively, under some conditions. We now specify such conditions in the following Assumption 1. For $m \in [2]$, let \mathbf{U}_m^* and \mathbf{V}_m^* be the true values of \mathbf{U}_m and \mathbf{V}_m from (7) and (9).

Assumption 1. For $m \in [2]$, let $\mathbf{U}_m^* \mathbf{V}_m^{*\top} = \mathbf{U}_m^{svd} \mathbf{V}_m^{svd\top}$ be a decomposition such that $\mathbf{U}_m^{svd\top} \mathbf{U}_m^{svd} = n \mathbf{I}_{d_m}$, $\mathbf{V}_m^{svd\top} \mathbf{V}_m^{svd} / nT$ is a diagonal matrix with decreasing entries, where $\mathbf{U}_m^{svd} \in \mathbb{R}^{n \times d_m}$ and $\mathbf{V}_m^{svd} \in \mathbb{R}^{nT \times d_m}$.

1. $\Theta^{*\top}\Theta^* = n\mathbf{I}_{k_1}$ and $\Phi^{*\top}\Phi^* = n\mathbf{I}_{k_2}$; $\Theta^* \perp \text{span}\{\mathbf{1}_n, \mathbf{U}_\beta^*\}$ and $\Phi^* \perp \text{span}\{\mathbf{1}_n, \mathbf{U}_\alpha^*\}$.
2. For $m \in [2]$, $\mathcal{M}_m(\mathcal{S}^*)\mathcal{M}_m(\mathcal{S}^*)^\top/T$ are diagonal matrices with strictly decreasing positive diagonals, and so do the limits as $T \rightarrow \infty$.
3. For $m \in [2]$, the diagonal entries of $\mathbf{V}_m^{svd\top}\mathbf{V}_m^{svd}/nT$ are positive and different, and so do the limits as $nT \rightarrow \infty$.
4. For $m \in [2]$, $\|\mathbf{U}_m^{svd}\|_{2 \rightarrow \infty} \leq C$ and $\|\mathbf{V}_m^{svd}\|_{2 \rightarrow \infty} \leq C$ for a constant C .

Remark 3. Conditions in Assumption 1 are standard and consistent with the literature of network analysis and tensor estimation (Xia et al., 2022; Li et al., 2023; Agterberg and Zhang, 2024; He et al., 2025). Note that \mathbf{U}_m^{svd} and \mathbf{V}_m^{svd} are the left and right singular matrices for $\mathbf{U}_m^*\mathbf{V}_m^{*\top}$ respectively after column scaling. The first condition in Assumption 1 requires that both columns of Θ^* and Φ^* are orthogonal and centered, and also orthogonal to column spaces of the intercept matrices, α^* and β^* , respectively. This is a crucial condition to identify Θ^* and Φ^* from \mathbf{U}_m^{svd} for $m \in [2]$. The second condition aims to fix the rotations after the column spaces of $\mathbf{J}_n\mathcal{M}_1(\mathcal{X})\mathbf{J}_{n,T}^\top$ and $\mathbf{J}_n\mathcal{M}_2(\mathcal{X})\mathbf{J}_{n,T}^\top$ are obtained. The third condition requires eigengaps between consecutive singular values of $\mathbf{U}_m^*\mathbf{V}_m^{*\top}$, which is a common assumption in the literature on matrix perturbation (Yu et al., 2015). The last condition in Assumption 1 assumes that each row of \mathbf{U}_m^{svd} and \mathbf{V}_m^{svd} are constrained in a compact set, which is also common and relates to the incoherence condition in matrix completion (Candes and Recht, 2012).

Under Assumption 1, the columns of Θ^* and Φ^* span the left singular subspaces of $\mathcal{M}_1(\mathcal{X}^*)$ and $\mathcal{M}_2(\mathcal{X}^*)$, respectively. We formalize this in Lemma 1.

Lemma 1. For $m \in [2]$, there exist ordered index subsets $S_m^* \subseteq [d_m]$ with $|S_m^*| = k_m$ and

diagonal sign matrices \mathbf{R}_m with entries in $\{\pm 1\}$ such that

$$\begin{aligned}\Theta^* &= [\mathbf{U}_1^{svd} \mathbf{R}_1]_{:,S_1^*}, & (\mathbf{I}_T \otimes \Phi^*) \mathcal{M}_1(\mathcal{S}^*)^\top &= [\mathbf{V}_1^{svd} \mathbf{R}_1]_{:,S_1^*}, \\ \Phi^* &= [\mathbf{U}_2^{svd} \mathbf{R}_2]_{:,S_2^*}, & (\mathbf{I}_T \otimes \Theta^*) \mathcal{M}_2(\mathcal{S}^*)^\top &= [\mathbf{V}_2^{svd} \mathbf{R}_2]_{:,S_2^*}.\end{aligned}$$

We now turn to \mathcal{S}^* . After recovering Θ^* and Φ^* , the $\mathcal{M}_1(\mathcal{S}^*)(\mathbf{I}_T \otimes \Phi^{*\top})$ and $\mathcal{M}_2(\mathcal{S}^*)(\mathbf{I}_T \otimes \Theta^{*\top})$ are also obtained, denoted by $(\mathbf{V}_1^{c*})^\top$ and $(\mathbf{V}_2^{c*})^\top$. The identifiability of \mathcal{S}^* is implied from the following relationship

$$(\mathbf{V}_1^{c*})^\top (\mathbf{I}_T \otimes \Phi^*) = \mathcal{M}_1(\mathcal{S}^*)(\mathbf{I}_T \otimes \Phi^{*\top})(\mathbf{I}_T \otimes \Phi^*) = \mathcal{M}_1(\mathcal{S}^*)(\mathbf{I}_T \otimes (\Phi^{*\top} \Phi)) = n \mathcal{M}_1(\mathcal{S}^*), \quad (11)$$

where the last equality is due to condition 2 in Assumption 1. We formalize the identifiability result in the following proposition.

Proposition 1. *Suppose Assumption 1 holds. For any set of parameters $(\check{\mathcal{X}}, \check{\Theta}, \check{\Phi}, \check{\mathcal{S}}, \check{\alpha}, \check{\beta})$ that satisfies (4), (5) and Assumption 1, if $\check{\mathcal{X}} = \mathcal{X}^*$, then $\check{\Theta} = \Theta^* \mathbf{R}_1$, $\check{\Phi} = \Phi^* \mathbf{R}_2$ and $\check{\mathcal{S}} = [\mathcal{S}^*; \mathbf{R}_1, \mathbf{R}_2, \mathbf{I}_T]$, where $\mathbf{R}_1 \in \mathbb{R}^{k_1 \times k_1}$ and $\mathbf{R}_2 \in \mathbb{R}^{k_2 \times k_2}$ are diagonal matrices with diagonal entries being ± 1 .*

Remark 4. *We give a discussion on the result of Proposition 1. First, we could only expect to identify Θ^* and Φ^* up to some column sign flipping, represented by \mathbf{R}_1 and \mathbf{R}_2 , which also appear in identifying \mathcal{S}^* . However, this sign uncertainty will not affect the inference task such as testing if $[\mathcal{S}^*]_{i,j,t} - [\mathcal{S}^*]_{i,j,t'} = 0$, for $i \in [k_1]$, $j \in [k_2]$ and $t \neq t'$. This is because \mathbf{R}_1 and \mathbf{R}_2 affect \mathcal{S}^* only through the first two modes. Detailed result is given in Section 3. Second, the challenging part in the current formulation (4) is the identification and estimation for the tensor components Θ^* , Φ^* and \mathcal{S}^* , which is new in the literature and that is what we will focus on in the following. The intercept parts, α^* and β^* , are more similar to previous factor analysis (Chen et al., 2020; Wang, 2022), so we here only focus*

on the new and more challenging parts of Θ^* , Φ^* and \mathcal{S}^* .

2.3 Estimation

According to (4), we need to estimate the loading matrices and core tensor from a tensor Tucker decomposition based on $\{y_{ijt}\}_{i,j \in [n], t \in [T]}$, which is a challenging task since a large-scale tensor optimization is highly non-convex and computationally intensive, especially when y_{ijt} 's are of different types. In the following, we propose a novel unfolding and fusion estimation procedure.

Let $\mathbf{Z}_m \in \mathbb{R}^{n \times nT}$ denote the mode- m unfolding of \mathcal{X} for $m \in [2]$. From (7) and (9), $\mathbf{Z}_m = \mathbf{U}_m \mathbf{V}_m^\top$. For $i \in [n]$ and $j \in [nT]$, let $\ell_{m,i,j}([\mathbf{Z}_m]_{i,j})$ denote the log-likelihood based on the observation $[\mathcal{M}_m(\mathcal{Y})]_{i,j}$ with $\mathcal{Y} = (y_{ijt})_{n \times n \times T}$ being the adjacency tensor. Then, for $m \in [2]$, the log-likelihood function corresponding to mode- m unfolding takes the form

$$L_m(\mathbf{Z}_m) = \sum_{i \in [n]} \sum_{j \in [nT]} \ell_{m,i,j}([\mathbf{Z}_m]_{i,j}). \quad (12)$$

We estimate $(\mathbf{U}_m, \mathbf{V}_m)$ by solving the following constrained maximum likelihood problem:

$$\begin{aligned} (\hat{\mathbf{U}}_m, \hat{\mathbf{V}}_m) &= \underset{\mathbf{U}_m, \mathbf{V}_m}{\operatorname{argmax}} L_m(\mathbf{U}_m \mathbf{V}_m^\top) \\ \text{subject to } & \|\mathbf{U}_m\|_{2 \rightarrow \infty} \leq C, \|\mathbf{V}_m\|_{2 \rightarrow \infty} \leq C, \\ & \mathbf{U}_m^\top \mathbf{U}_m = n \mathbf{I}_{d_m}, \\ & \mathbf{V}_m^\top \mathbf{V}_m \text{ is diagonal with decreasing entries.} \end{aligned} \quad (13)$$

Remark 5. Note that the log-likelihood function L_m depends on $(\mathbf{U}_m, \mathbf{V}_m)$ only through $\mathbf{U}_m \mathbf{V}_m^\top$. Therefore, we could rotate \mathbf{U}_m and \mathbf{V}_m simultaneously by multiplying an orthogonal matrix without changing the value of L_m . The last two constraints in (13) are to fix the rotation. We also require each row of \mathbf{U}_m and \mathbf{V}_m lies within a compact set. Similar

constraints have been adopted in the literature of factor analysis (Bai, 2003; Wang, 2022).

Based on (10), we further apply two-sided centering to $\widehat{\mathbf{Z}}_m = \widehat{\mathbf{U}}_m \widehat{\mathbf{V}}_m^\top$ to get $\mathbf{J}_n \widehat{\mathbf{Z}}_m \mathbf{J}_{n,T}^\top$. Then, we identify the columns of $\widehat{\mathbf{U}}_1$ and $\widehat{\mathbf{U}}_2$ which correspond to Θ and Φ respectively by choosing the k_m largest norm of columns after projection onto the column space of $\mathbf{J}_n \widehat{\mathbf{Z}}_m \mathbf{J}_{n,T}^\top$. The $\widehat{\Theta}$ and $\widehat{\Phi}$ are obtained by selecting such columns from $\widehat{\mathbf{U}}_1$ and $\widehat{\mathbf{U}}_2$, respectively. Finally, the $\{\widehat{\Lambda}_t\}_{t=1}^T$ is estimated according to (11). We summarize the estimation procedure in Algorithm 1 below.

Algorithm 1 Estimating latent positions and connection matrices by *unfolding and fusion*.

Input: Adjacency tensor $\mathcal{Y} = (y_{ijt})_{n \times n \times T}$, link functions $\{g_{ijt}(\cdot) : i, j \in [n], t \in [T]\}$, dimensions d_1, d_2, k_1, k_2 .

1: **for** $m = 1, 2$ **do**

2: Obtain $(\widehat{\mathbf{U}}_m, \widehat{\mathbf{V}}_m)$ from the constrained maximum likelihood optimization (13) based on mode- m unfolding.

3: Form $\widehat{\mathbf{Z}}_m = \widehat{\mathbf{U}}_m \widehat{\mathbf{V}}_m^\top$ and its centered version $\widehat{\mathbf{Z}}_m^c = \mathbf{J}_n \widehat{\mathbf{Z}}_m \mathbf{J}_{n,T}^\top$. Define $\mathbf{P}_m \in \mathbb{R}^{n \times n}$ as the projection matrix onto the column space of $\widehat{\mathbf{Z}}_m^c$.

4: For each $j = [d_m]$, compute the projection norm $s_{m,j} = \|\mathbf{P}_m \widehat{\mathbf{U}}_m[:,j]\|_2$. Select \widehat{S}_m as the ordered index set corresponding to the k_m largest values among $\{s_{m,j}\}$, and arrange the elements of \widehat{S}_m such that the diagonals of $[\widehat{\mathbf{V}}_m]_{:, \widehat{S}_m}^\top [\widehat{\mathbf{V}}_m]_{:, \widehat{S}_m}$ is in decreasing order.

5: Set $\widehat{\mathbf{U}}_m^c = [\widehat{\mathbf{U}}_m]_{:, \widehat{S}_m}$, $\widehat{\mathbf{V}}_m^c = [\widehat{\mathbf{V}}_m]_{:, \widehat{S}_m}$, and $\widehat{\mathcal{S}} \in \mathbb{R}^{k_1 \times k_2 \times T}$ by

$$\mathcal{M}_1(\widehat{\mathcal{S}}) = (\widehat{\mathbf{V}}_1^c)^\top (\mathbf{I}_T \otimes \widehat{\mathbf{U}}_2^c) / n.$$

6: **end for**

7: Set $\widehat{\Theta} = \widehat{\mathbf{U}}_1^c$, $\widehat{\Phi} = \widehat{\mathbf{U}}_2^c$ and $\{\widehat{\Lambda}_t\}_{t=1}^T$ with $\widehat{\Lambda}_t = \widehat{\mathcal{S}}_{:, :, t}$.

Output: $\{\widehat{\Theta}, \widehat{\Phi}, \{\widehat{\Lambda}_t\}_{t=1}^T, \{\widehat{\mathbf{V}}_m^c\}_{m \in [2]}, \{\widehat{S}_m\}_{m \in [2]}\}$

To estimate the latent positions, Algorithm 1 solves two constrained maximum likelihood optimizations regarding low rank matrices through tensor unfolding. This enables us to utilize the rich literature of factor analysis and low rank matrix estimation. Specifically, there exist consistent initial values by spectral methods for different data types (Bai, 2003; Zhang et al., 2020a; He et al., 2025). This is in sharp contrast to solving an optimization for a large-scale tensor, which is highly non-convex and hard to find consistent initial values,

especially for non-continuous edge types (Han et al., 2022). Furthermore, by tensor unfolding, the dimensions d_1, d_2 could be consistently estimated (Zhang et al., 2020a; Chen and Li, 2022). In practice, k_1, k_2 could be chosen by the scree plots for singular values of $\widehat{\mathbf{Z}}_m^c$ for $m \in [2]$. Finally, Algorithm 1 estimates the connection matrices, which correspond to the core tensor in the Tucker decomposition, by a fusion operator which involves only matrix multiplication. This is not only computationally fast, but also facilitates us to derive the asymptotic distribution of the estimator. More details are deferred to Section 3.2.

3 Theory

In this section, we establish the convergence rates and asymptotic distributions for the latent position and the connection matrix estimators, which further facilitate statistical inference tasks for multilayer networks.

3.1 Asymptotics for the latent position estimators

For $m \in [2], i \in [n]$ and $j \in [nT]$, denote $\pi_{m,i,j}^* = [\mathcal{M}_m(\mathcal{X}^*)]_{i,j}$. We impose the following regularity conditions on the likelihood functions.

Assumption 2. *For any given compact domain Π , there exists $M > 0$ such that for all $m \in [2], i \in [n], j \in [nT]$: 1, there exist $0 < b_L < b_U$ such that $b_L \leq -\frac{\partial^2 \ell_{m,i,j}(\pi)}{\partial \pi^2} \leq b_U$ for all $\pi \in \Pi$; 2, $\sup_{\pi \in \Pi} \left| \frac{\partial^3 \ell_{m,i,j}(\pi)}{\partial \pi^3} \right| \leq M$; 3, $\left\| \frac{\partial \ell_{m,i,j}(\pi_{m,i,j}^*)}{\partial \pi} \right\|_{\psi_1} \leq M$.*

Remark 6. *Assumption 2 specifies smoothness conditions on the individual log-likelihood function $\ell_{m,i,j}(\cdot)$, which are commonly used in the literature (Bai, 2003; Wang, 2022). The first and second conditions in Assumption 2 ensure the concavity for each $\ell_{m,i,j}(\cdot)$ and the boundedness of its third order derivative, when true parameters lie in a compact set. The third condition states that the score functions are sub-exponential, which is important in*

establishing the error bounds for the estimators. Assumption 2 holds for many types of $g_{ijt}(\cdot | x_{ijt})$ in (2), including linear, logistic, Probit, and Poisson models.

We now study the asymptotic behavior of $\widehat{\mathbf{U}}_m$ and $\widehat{\mathbf{V}}_m$ for $m \in [2]$. The following Theorem 1 establishes the uniform convergence for the estimated latent positions.

Theorem 1. *Suppose Assumptions 1-2 hold, and as $n \rightarrow \infty$, $(T^{1+\epsilon}/n) \rightarrow 0$ for some small $\epsilon > 0$, then*

$$\|\widehat{\Theta} - \Theta^* \mathbf{R}_1\|_F^2 = O_p\left(\frac{1}{T}\right), \quad \|\widehat{\Phi} - \Phi^* \mathbf{R}_2\|_F^2 = O_p\left(\frac{1}{T}\right), \quad (14)$$

where $\mathbf{R}_m \in \mathbb{R}^{k_m \times k_m}$ are diagonal with entries in ± 1 . Moreover, the uniform convergence rates for individualized estimation error are

$$\|\widehat{\Theta} - \Theta^* \mathbf{R}_1\|_{2 \rightarrow \infty} = O_p\left(\frac{\log n}{\sqrt{nT}}\right), \quad \|\widehat{\Phi} - \Phi^* \mathbf{R}_2\|_{2 \rightarrow \infty} = O_p\left(\frac{\log n}{\sqrt{nT}}\right).$$

Remark 7. *The convergence rates for the latent positions estimators in Frobenius norm are consistent with Arroyo et al. (2021) and He et al. (2025), both of which focus on undirected multilayer networks. (14) is also consistent with the result in Zhang et al. (2020b) in the special case when there are no degree heterogeneity parameters. Theorem 1 further establishes the uniform convergence rates for the latent positions estimation errors. When $T = 1$, the rate becomes $O_p(n^{-1/2} \log n)$, and is slightly faster than the rate derived in Li et al. (2023) for single layer latent space model, which is $O_p(n^{-1/2+\eta})$ for arbitrarily small $\eta > 0$.*

We now focus on the asymptotic distributions of $[\widehat{\Theta}]_{i,:}$ and $[\widehat{\Phi}]_{i,:}$ for $i \in [n]$. Recall the definitions of $\mathbf{U}_m^{svd}, \mathbf{V}_m^{svd}$ in Assumption 1. For $m \in [2]$, we further define $\mathbf{u}_m^{svd} = \text{vec}((\mathbf{U}_m^{svd})^\top)$ and $\mathbf{v}_m^{svd} = \text{vec}((\mathbf{V}_m^{svd})^\top)$, such that

$$\begin{aligned} \mathbf{u}_m^{svd} &= ([\mathbf{u}_m^{svd}]_1^\top, \dots, [\mathbf{u}_m^{svd}]_n^\top)^\top \in \mathbb{R}^{nd_m}, \\ \mathbf{v}_m^{svd} &= ([\mathbf{v}_m^{svd}]_1^\top, \dots, [\mathbf{v}_m^{svd}]_{nT}^\top)^\top \in \mathbb{R}^{nTd_m}, \end{aligned} \quad (15)$$

where $[\mathbf{u}_m^{svd}]_s^\top, [\mathbf{v}_m^{svd}]_s^\top \in \mathbb{R}^{1 \times d_m}$ are the s -th rows of \mathbf{U}_m^{svd} and \mathbf{V}_m^{svd} , respectively. For any $i \in [n], j \in [nT]$, denote

$$\Sigma_{\mathbf{u}_m^{svd}, j} := \sum_{s \in [n]} \left(-\frac{\partial^2 \ell_{m,s,j}(\pi_{m,s,j}^*)}{\partial \pi_{m,s,j}^2} \right) [\mathbf{u}_m^{svd}]_s [\mathbf{u}_m^{svd}]_s^\top, \quad \Omega_{\mathbf{u}_m^{svd}, j} := \sum_{s \in [n]} \left(\frac{\partial \ell_{m,s,j}(\pi_{m,s,j}^*)}{\partial \pi_{m,s,j}} \right)^2 [\mathbf{u}_m^{svd}]_s [\mathbf{u}_m^{svd}]_s^\top, \quad (16)$$

$$\Sigma_{\mathbf{v}_m^{svd}, i} := \sum_{s \in [nT]} \left(-\frac{\partial^2 \ell_{m,i,s}(\pi_{m,i,s}^*)}{\partial \pi_{m,i,s}^2} \right) [\mathbf{v}_m^{svd}]_s [\mathbf{v}_m^{svd}]_s^\top, \quad \Omega_{\mathbf{v}_m^{svd}, i} := \sum_{s \in [nT]} \left(\frac{\partial \ell_{m,i,s}(\pi_{m,i,s}^*)}{\partial \pi_{m,i,s}} \right)^2 [\mathbf{v}_m^{svd}]_s [\mathbf{v}_m^{svd}]_s^\top. \quad (17)$$

The following Theorem 2 establishes the asymptotic distributions for $[\widehat{\Theta}]_{i,:}$ and $[\widehat{\Phi}]_{i,:}$, which is the basis for constructing the confidence regions for the latent positions, and also important for deriving the asymptotic distributions for the estimated connection matrices.

Theorem 2. *Suppose Assumptions 1-2 hold and as $n \rightarrow \infty$, $(T^{1+\epsilon}/n) \rightarrow 0$ for some small $\epsilon > 0$. Then, for $i \in [n]$, up to diagonal sign matrices \mathbf{R}_m , we have*

$$\left([\Sigma_{\mathbf{v}_1^{svd}, i}^{-1} \Omega_{\mathbf{v}_1^{svd}, i} \Sigma_{\mathbf{v}_1^{svd}, i}^{-1}]_{S_1^*, S_1^*} \right)^{-\frac{1}{2}} \left([\widehat{\Theta}]_{i,:}^\top - [\Theta^* \mathbf{R}_1]_{i,:}^\top \right) \xrightarrow{d} N(\mathbf{0}, \mathbf{I}_{k_1}),$$

$$\left([\Sigma_{\mathbf{v}_2^{svd}, i}^{-1} \Omega_{\mathbf{v}_2^{svd}, i} \Sigma_{\mathbf{v}_2^{svd}, i}^{-1}]_{S_2^*, S_2^*} \right)^{-\frac{1}{2}} \left([\widehat{\Phi}]_{i,:}^\top - [\Phi^* \mathbf{R}_2]_{i,:}^\top \right) \xrightarrow{d} N(\mathbf{0}, \mathbf{I}_{k_2}).$$

Moreover, for $m \in [2]$ and $j \in [nT]$,

$$\left([\Sigma_{\mathbf{u}_m^{svd}, j}^{-1} \Omega_{\mathbf{u}_m^{svd}, j} \Sigma_{\mathbf{u}_m^{svd}, j}^{-1}]_{S_m^*, S_m^*} \right)^{-\frac{1}{2}} \left([\widehat{\mathbf{V}}_m^c]_{j,:}^\top - [\mathbf{V}_m^{c*} \mathbf{R}_m]_{j,:}^\top \right) \xrightarrow{d} N(\mathbf{0}, \mathbf{I}_{k_m}).$$

Remark 8. *The key challenge in establishing asymptotic normality for $[\widehat{\Theta}]_{i,:}$ and $[\widehat{\Phi}]_{i,:}$ relates to the identifiability issue discussed in Section 2.2. Specifically, we can change $(\mathbf{U}_m, \mathbf{V}_m)$ to $(\mathbf{U}_m \mathbf{Q}, \mathbf{V}_m (\mathbf{Q}^{-1})^\top)$ for any invertible matrix $\mathbf{Q} \in \mathbb{R}^{k_m \times k_m}$, while the value of L_m remains unchanged. This will result in a singular Hessian matrix if we treat L_m as a function of both \mathbf{U}_m and \mathbf{V}_m , which makes the standard theory of M-estimation fail. To solve this, we reformulate the constraints in (13) as a Lagrange dual problem and analyze the corresponding Hessian matrix for the Lagrangian regularized log likelihood function. Similar techniques have*

been adopted in [Wang \(2022\)](#) and [Li et al. \(2023\)](#) under different model settings. However, the tensor structure in (4) requires more complicated identifiability conditions as discussed in [Section 2.2](#) and [Assumption 1](#), making it more challenging to derive the asymptotic distributions for the estimators.

Remark 9. *Theorem 2 implies that both $[\widehat{\Theta}]_{i,:}$ and $[\widehat{\Phi}]_{i,:}$ are oracle estimators. Specifically, the asymptotic covariance matrix of $[\widehat{\Theta}]_{i,:}$, which is $\Sigma_{\mathbf{v}_1^{svd},i}^{-1}$, matches with the Cramér-Rao lower bound for estimating $[\Theta^*]_{i,:}$ in the scenario when all other parameters $\{[\Theta^*]_{j,:}\}_{j \neq i}$, Φ^* , $\{\Lambda_t^*\}_{t=1}^T$, α^* and β^* are known. Similar property holds for $[\widehat{\Phi}]_{i,:}$.*

The asymptotic covariance matrices of $\widehat{\Theta}$ and $\widehat{\Phi}$ can be estimated via plug-in estimators. Define $\widehat{\mathbf{u}}_m := \text{vec}(\widehat{\mathbf{U}}_m^\top)$, $\widehat{\mathbf{v}}_m := \text{vec}(\widehat{\mathbf{V}}_m^\top)$. The following [Corollary 1](#) provides a guide for constructing confidence regions for $[\Theta^*]_{i,:}$ and $[\Phi^*]_{i,:}$ up to sign flipping.

Corollary 1. *Under the conditions of [Theorem 2](#), for $m \in [2]$, $i \in [n]$, and $j \in [nT]$, define $\widehat{\pi}_{m,i,j} := [\mathcal{M}_m(\widehat{\mathcal{X}})]_{i,j}$ and*

$$\widehat{\Sigma}_{\widehat{\mathbf{v}}_m,i} := \sum_{s \in [nT]} \left(-\frac{\partial^2 \ell_{m,i,s}(\widehat{\pi}_{m,i,s})}{\partial \pi_{m,i,s}^2} \right) [\widehat{\mathbf{v}}_m]_s [\widehat{\mathbf{v}}_m]_s^\top, \quad \widehat{\Omega}_{\widehat{\mathbf{v}}_m,i} := \sum_{s \in [nT]} \left(\frac{\partial \ell_{m,i,s}(\widehat{\pi}_{m,i,s})}{\partial \pi_{m,i,s}} \right)^2 [\widehat{\mathbf{v}}_m]_s [\widehat{\mathbf{v}}_m]_s^\top.$$

As $n \rightarrow \infty$, $\widehat{\Sigma}_{\widehat{\mathbf{v}}_m,i}$ and $\widehat{\Omega}_{\widehat{\mathbf{v}}_m,i}$ are consistent estimators of $\Sigma_{\mathbf{v}_m^{svd},i}$ and $\Omega_{\mathbf{v}_m^{svd},i}$, respectively. Let \widehat{S}_m be the ordered index sets from [Algorithm 1](#). Moreover,

$$\begin{aligned} & \left([\widehat{\Sigma}_{\widehat{\mathbf{v}}_1,i}^{-1} \widehat{\Omega}_{\widehat{\mathbf{v}}_1,i} \widehat{\Sigma}_{\widehat{\mathbf{v}}_1,i}^{-1}]_{\widehat{S}_1, \widehat{S}_1} \right)^{-\frac{1}{2}} \left([\widehat{\Theta}]_{i,:}^\top - [\Theta^* \mathbf{R}_1]_{i,:}^\top \right) \xrightarrow{d} N(\mathbf{0}, \mathbf{I}_{k_1 \times k_1}), \\ & \left([\widehat{\Sigma}_{\widehat{\mathbf{v}}_2,i}^{-1} \widehat{\Omega}_{\widehat{\mathbf{v}}_2,i} \widehat{\Sigma}_{\widehat{\mathbf{v}}_2,i}^{-1}]_{\widehat{S}_2, \widehat{S}_2} \right)^{-\frac{1}{2}} \left([\widehat{\Phi}]_{i,:}^\top - [\Phi^* \mathbf{R}_2]_{i,:}^\top \right) \xrightarrow{d} N(\mathbf{0}, \mathbf{I}_{k_2 \times k_2}). \end{aligned}$$

[Corollary 1](#) enables the construction of confidence regions for the latent position estimators. It further supports inference problems such as testing whether two nodes belong to the same community and network assisted regression.

3.2 Asymptotics for the connection matrix estimators

We now establish the asymptotic distributions for the connection matrix estimators, and show how to perform hypothesis testing on whether the structures for two specific network layers are the same, which is a typical inference task for multilayer networks and has not been established in the literature yet.

Recall the connection matrix estimators in Algorithm 1, we have

$$\begin{aligned} [\widehat{\Lambda}_t]_{i,j} &= \widehat{\mathcal{S}}_{i,j,t} = \left[\mathcal{M}_1(\widehat{\mathcal{S}}) \right]_{i,j+k_2(t-1)} \\ &= \frac{1}{n} \sum_{s=1}^{nT} \left([\widehat{\mathbf{V}}_1^c]_{s,i} \cdot [\mathbf{I}_T \otimes \widehat{\Phi}]_{s,j+k_2(t-1)} \right). \end{aligned} \quad (18)$$

Theorem 3 establishes a uniform convergence rate for $[\widehat{\Lambda}_t]_{i,j}$ with $(i, j, t) \in [k_1] \times [k_2] \times [T]$.

Theorem 3. *Under Assumptions 1-2, as $(n, T) \rightarrow \infty$ with $(T^{1+\epsilon}/n) \rightarrow 0$ for some $\epsilon > 0$,*

$$\max_{t \in [T]} \|\widehat{\Lambda}_t - \mathbf{R}_1 \Lambda_t^* \mathbf{R}_2\|_{\max} = O_p \left(\frac{\log T}{n} \right),$$

where \mathbf{R}_m are diagonal matrices with entries ± 1 defined in Theorem 1.

Remark 10. *The term $\log T$ in the upper bound in Theorem 3 comes from the maximization over T asymptotic independent terms $\widehat{\Lambda}_t - \mathbf{R}_1 \Lambda_t^* \mathbf{R}_2$, each of which is of $O_p(n^{-1})$. This is consistent with the convergence rate derived in Arroyo et al. (2021), which focused on undirected networks and assumed a linear model with additive noises. Note that if $\Theta^*, \Phi^*, \alpha^*, \beta^*$ are known and fixed, then we have n^2 independent edges $\{y_{ijt}\}_{i,j \in [n]}$ to estimate Λ_t^* , and the oracle error rate should be $O_p(n^{-1})$.*

We now turn to the asymptotic distributions for $[\widehat{\Lambda}_t]_{i,j}$, leveraging the first-order expansions of $\widehat{\mathbf{V}}_1^c$ and $\widehat{\Phi}$. For $m \in [2]$, define the projection matrices $\mathbf{P}_{S_m^*} \in \mathbb{R}^{k_m \times d_m}$ as $\mathbf{P}_{S_m^*} = (\mathbf{e}_{j_1} \cdots \mathbf{e}_{j_{k_m}})^\top \in \mathbb{R}^{k_m \times d_m}$, where $S_m^* = \{j_1, \dots, j_{k_m}\}$ with $j_1 < \cdots < j_{k_m}$ and \mathbf{e}_i

denotes the i -th canonical basis vector in \mathbb{R}^{d_m} . For any vector $\mathbf{u} \in \mathbb{R}^{d_m}$, $\mathbf{P}_{S_m^*} \mathbf{u}$ is the sub-vector of \mathbf{u} with indices in S_m^* . By expansion (18), we formalize the asymptotic distribution of $[\widehat{\Lambda}_t]_{i,j}$ as follows.

Theorem 4. *Under Assumptions 1-2, for each fixed triple $(i, j, t) \in [k_1] \times [k_2] \times [T]$, as $(n, T) \rightarrow \infty$ with $(T^{1+\epsilon}/n) \rightarrow 0$ for some small $\epsilon > 0$, we have*

$$\sigma_{i,j,t}^{-1} \left([\widehat{\Lambda}_t]_{i,j} - [\mathbf{R}_1 \Lambda_t^* \mathbf{R}_2]_{i,j} \right) \xrightarrow{d} N(0, 1),$$

where

$$\sigma_{i,j,t}^2 := \frac{1}{n^2} \sum_{s=1}^n [\mathbf{P}_{S_2^*} [\mathbf{u}_2^{svd}]_s]_j^2 \cdot \left([[\Sigma_{\mathbf{u}_1^{svd}, s+n(t-1)}^{-1} \Omega_{\mathbf{u}_1^{svd}, s+n(t-1)} \Sigma_{\mathbf{u}_1^{svd}, s+n(t-1)}^{-1}]_{S_1^*, S_1^*}]_{i,i} \right).$$

Furthermore, the asymptotic normality still holds if we replace $\sigma_{i,j,t}^2$ with $\widehat{\sigma}_{i,j,t}^2$ defined by

$$\widehat{\sigma}_{i,j,t}^2 = \frac{1}{n^2} \sum_{s=1}^n [\mathbf{P}_{\widehat{S}_2} [\widehat{\mathbf{u}}_2]_s]_j^2 \cdot \left([[\widehat{\Sigma}_{\widehat{\mathbf{u}}_1, s+n(t-1)}^{-1} \widehat{\Omega}_{\widehat{\mathbf{u}}_1, s+n(t-1)} \widehat{\Sigma}_{\widehat{\mathbf{u}}_1, s+n(t-1)}^{-1}]_{\widehat{S}_1, \widehat{S}_1}]_{i,i} \right). \quad (19)$$

In many applications, we need to test whether two network layers have the same structure. For example, for a dynamic network, we want to test whether there is a structural change at a specific time point. To do this, we need to partial out the effect of degree heterogeneity across different layers. Then, based on (3), this is equivalent to test

$$H_0^{(t,t')} : \Lambda_t^* = \Lambda_{t'}^* \quad v.s. \quad H_1^{(t,t')} : \Lambda_t^* \neq \Lambda_{t'}^*, \quad (20)$$

for $t \neq t' \in [T]$. To test (20), we first consider the following element-wise hypothesis:

$$H_0^{(i,j,t,t')} : [\Lambda_t^*]_{i,j} = [\Lambda_{t'}^*]_{i,j} \quad v.s. \quad H_1^{(i,j,t,t')} : [\Lambda_t^*]_{i,j} \neq [\Lambda_{t'}^*]_{i,j} \quad (21)$$

for some $(i, j) \in [k_1] \times [k_2]$ and $t \neq t' \in [T]$. To this end, we require the following corollary.

Corollary 2. *Under the conditions of Theorem 4, for $(i, j) \in [k_1] \times [k_2]$ and $t \neq t' \in [T]$, the asymptotic joint distribution of $([\widehat{\Lambda}_t]_{i,j}, [\widehat{\Lambda}_{t'}]_{i,j})$ is given by*

$$\begin{pmatrix} \widehat{\sigma}_{i,j,t}^{-1} & 0 \\ 0 & \widehat{\sigma}_{i,j,t'}^{-1} \end{pmatrix} \begin{pmatrix} [\widehat{\Lambda}_t]_{i,j} - [\mathbf{R}_1 \Lambda_t^* \mathbf{R}_2]_{i,j} \\ [\widehat{\Lambda}_{t'}]_{i,j} - [\mathbf{R}_1 \Lambda_{t'}^* \mathbf{R}_2]_{i,j} \end{pmatrix} \xrightarrow{d} N(\mathbf{0}, \mathbf{I}_2). \quad (22)$$

Let $\widehat{\delta}_{i,j,t,t'} := ([\widehat{\Lambda}_t]_{i,j} - [\widehat{\Lambda}_{t'}]_{i,j})$ and $\delta_{i,j,t,t'}^* := ([\mathbf{R}_1 \Lambda_t^* \mathbf{R}_2]_{i,j} - [\mathbf{R}_1 \Lambda_{t'}^* \mathbf{R}_2]_{i,j})$, then

$$\left(\widehat{\sigma}_{i,j,t}^2 + \widehat{\sigma}_{i,j,t'}^2\right)^{-\frac{1}{2}} \left(\widehat{\delta}_{i,j,t,t'} - \delta_{i,j,t,t'}^*\right) \xrightarrow{d} N(0, 1) \quad (23)$$

where $\widehat{\sigma}_{i,j,t}, \widehat{\sigma}_{i,j,t'}$ are defined in (19).

By (23), we could construct the confidence interval for $\widehat{\delta}_{i,j,t,t'}$ and further test (21) by checking whether or not the confidence interval at specific level contains zero. In particular, we reject $H_0^{(i,j,t,t')}$ at level $1 - \alpha$ if $|\widehat{\delta}_{i,j,t,t'}| > q_{1-\alpha/2} \left(\widehat{\sigma}_{i,j,t}^2 + \widehat{\sigma}_{i,j,t'}^2\right)^{\frac{1}{2}}$, where $q_{1-\alpha/2}$ is the $1 - \alpha/2$ quantile for standard normal distribution. We could further test (20) by the method of Bonferroni correction. Specifically, we reject $H_0^{(t,t')}$ at level $1 - \alpha$ if $|\widehat{\delta}_{i,j,t,t'}| > q_{1-\alpha/(2k_1k_2)} \left(\widehat{\sigma}_{i,j,t}^2 + \widehat{\sigma}_{i,j,t'}^2\right)^{\frac{1}{2}}$ for some $(i, j) \in [k_1] \times [k_2]$. Alternatively, false discovery rate (FDR) control procedures can be readily applied to account for multiple testing.

4 Numerical experiments

4.1 Simulation examples

We conduct simulation studies to evaluate the finite-sample performance of our estimators and to examine the accuracy of the asymptotic normal approximations derived in Section 3. For each simulation setting, we vary the number of nodes $n \in \{400, 800, 1200, 1600\}$ and

the number of layers $T \in \{50, 100\}$. The latent dimensions are fixed at $k_1 = k_2 = 3$ and $k_\alpha = k_\beta = 2$. The parameters $\Theta^*, \Phi^*, \{\Lambda_t^*\}_{t=1}^T, \mathbf{U}_\alpha^*, \mathbf{U}_\beta^*, \mathbf{V}_\alpha^*, \mathbf{V}_\beta^*$ are generated according to Assumption 1.

Specifically, to construct the latent positions and degree heterogeneity parameters, we first generate an $n \times (k_1 + k_\beta)$ matrix and an $n \times (k_2 + k_\alpha)$ matrix with entries drawn independently from a standard Gaussian distribution. Then, Θ^* and Φ^* are constructed as centered orthogonal bases by applying QR decomposition to the first k_1 and k_2 columns of the two random matrices. The factors \mathbf{U}_β^* and \mathbf{U}_α^* are then constructed by projecting the remaining columns onto the orthogonal complements of Θ^* and Φ^* , respectively. Meanwhile, the matrices \mathbf{V}_β^* and \mathbf{V}_α^* are generated independently by applying singular value decomposition to two random matrices with independent standard normal entries. Furthermore, for each $t \in [T]$, the connection matrix Λ_t^* is constructed as a diagonal matrix with decreasing entries that are generated randomly from normal distribution.

We consider three types of networks: continuous, count-valued and binary, which are generated by Gaussian, Poisson and logistic models specified in Remark 1, respectively. The estimation accuracies of the latent positions and connection matrices are evaluated by $\Delta\Theta := \|\widehat{\Theta} - \Theta^* \mathbf{R}_1\|_{2 \rightarrow \infty}$, $\Delta\Phi := \|\widehat{\Phi} - \Phi^* \mathbf{R}_2\|_{2 \rightarrow \infty}$ and $\Delta\Lambda = \max_{t \in [T]} \|\widehat{\Lambda}_t - \mathbf{R}_1 \Lambda_t \mathbf{R}_2\|_{\max}$. To assess the asymptotic distributions for $\widehat{\Theta}$, $\widehat{\Phi}$, and $\{\widehat{\Lambda}_t\}_{t=1}^T$, we examine three representative parameters: $[\widehat{\Theta}]_{1,1}$, $[\widehat{\Phi}]_{1,1}$, and $[\widehat{\Lambda}_1]_{1,1}$ and report the coverage rates of the confidence interval over 200 independent experiments.

The results are summarized in Figure 1 and Table 1. Figure 1 shows the estimation errors of $\widehat{\Theta}$, $\widehat{\Phi}$ and $\{\widehat{\Lambda}_t\}_{t=1}^T$ under different settings, which clearly decrease as n, T grow. In addition, $\widehat{\Theta}$ and $\widehat{\Phi}$ exhibit comparable rates of decay across different values of n and T , whereas $\widehat{\Lambda}_t$ converges at a noticeably faster rate. These empirical results are consistent with the theoretical results established in Theorem 1 and Theorem 3. Table 1 further shows the coverage rates of the confidence intervals at level 95% for the three parameters over

Parameter	Setting	$n = 400$	$n = 800$	$n = 1200$	$n = 1600$
$[\Theta]_{1,1}$	Gaussian	0.950 (0.0154)	0.955 (0.0147)	0.915 (0.0197)	0.960 (0.0139)
	Poisson	0.860 (0.0245)	0.950 (0.0154)	0.920 (0.0191)	0.955 (0.0147)
	Binary	0.905 (0.0207)	0.910 (0.0202)	0.915 (0.0197)	0.920 (0.0191)
$[\Phi]_{1,1}$	Gaussian	0.975 (0.0110)	0.955 (0.0147)	0.960 (0.0139)	0.950 (0.0154)
	Poisson	0.935 (0.0174)	0.930 (0.0180)	0.947 (0.0158)	0.960 (0.0139)
	Binary	0.980 (0.0099)	0.940 (0.0168)	0.925 (0.0186)	0.950 (0.0154)
$[\Lambda_1]_{1,1}$	Gaussian	0.955 (0.0147)	0.925 (0.0186)	0.950 (0.0154)	0.950 (0.0154)
	Poisson	0.930 (0.0180)	0.960 (0.0139)	0.940 (0.0168)	0.955 (0.0147)
	Binary	0.920 (0.0192)	0.900 (0.0212)	0.890 (0.0221)	0.915 (0.0197)

(a) $T = 50$

Parameter	Setting	$n = 400$	$n = 800$	$n = 1200$	$n = 1600$
$[\Theta]_{1,1}$	Gaussian	0.970 (0.0121)	0.970 (0.0121)	0.945 (0.0161)	0.940 (0.0168)
	Poisson	0.930 (0.0180)	0.945 (0.0161)	0.945 (0.0161)	0.925 (0.0186)
	Binary	0.865 (0.0242)	0.925 (0.0186)	0.925 (0.0186)	0.910 (0.0202)
$[\Phi]_{1,1}$	Gaussian	0.935 (0.0174)	0.950 (0.0154)	0.980 (0.0099)	0.955 (0.0147)
	Poisson	0.940 (0.0168)	0.905 (0.0207)	0.945 (0.0161)	0.945 (0.0161)
	Binary	0.835 (0.0263)	0.915 (0.0197)	0.930 (0.0180)	0.945 (0.0161)
$[\Lambda_1]_{1,1}$	Gaussian	0.945 (0.0161)	0.955 (0.0147)	0.950 (0.0154)	0.950 (0.0154)
	Poisson	0.915 (0.0197)	0.950 (0.0154)	0.945 (0.0161)	0.950 (0.0154)
	Binary	0.930 (0.0180)	0.905 (0.0207)	0.915 (0.0197)	0.905 (0.0207)

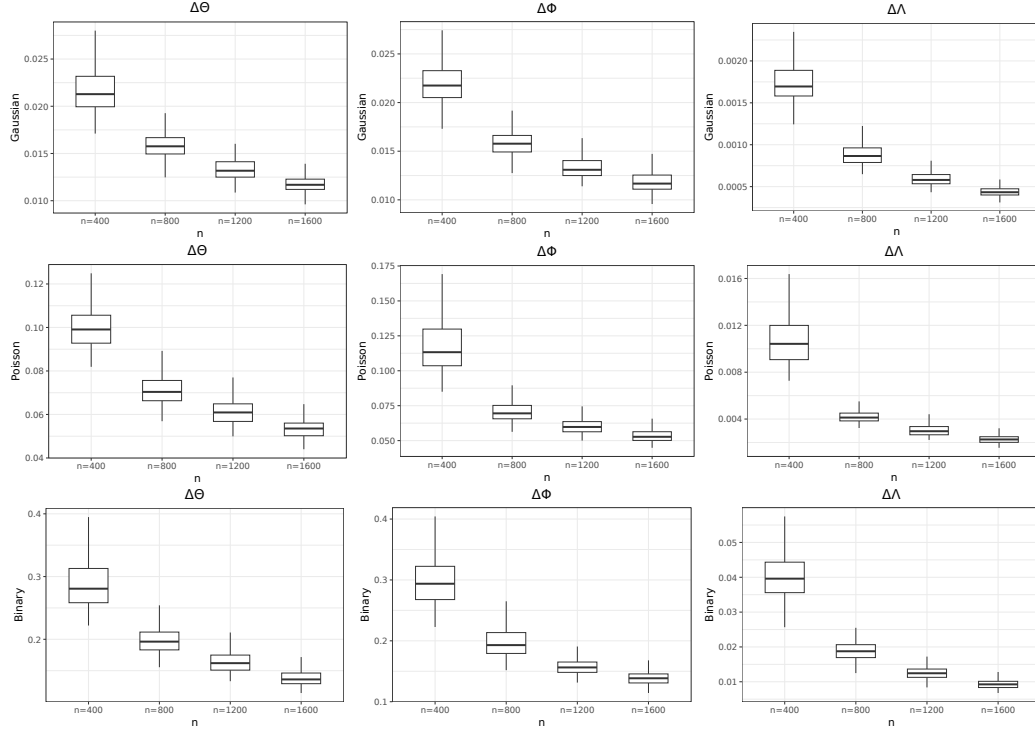
(b) $T = 100$

Table 1: Coverage rates of 95% confidence intervals for $[\Theta^*]_{1,1}$ and $[\Phi^*]_{1,1}$ and $[\Lambda_1^*]_{1,1}$ over 200 independent experiments under different settings and n, T . Standard errors are reported in parentheses.

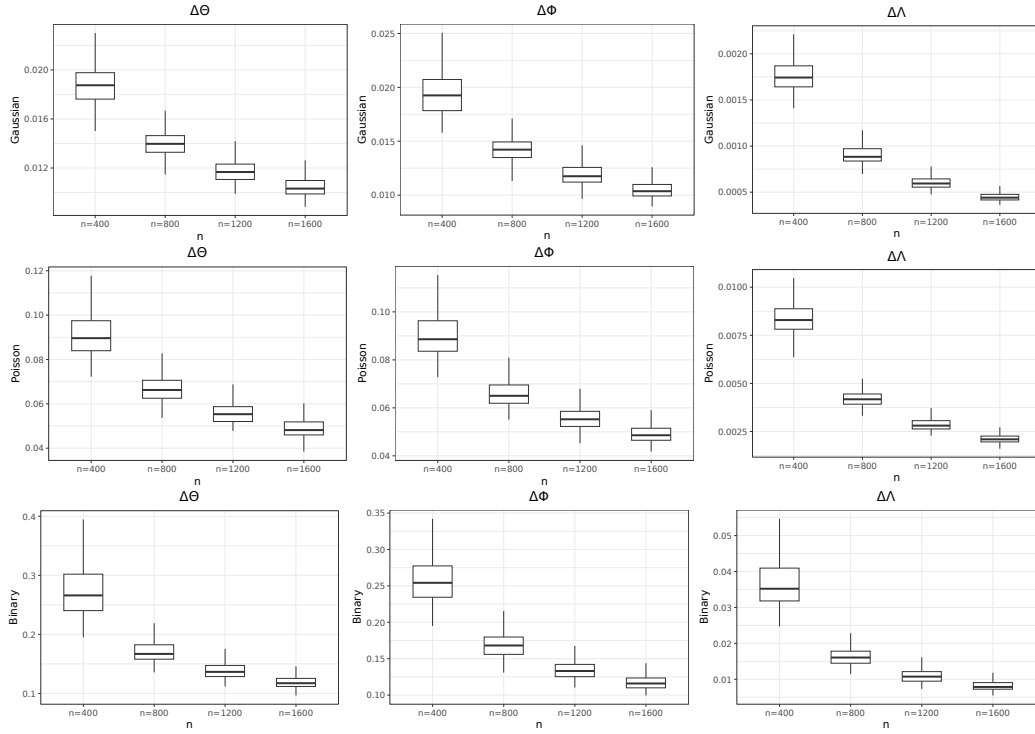
200 independent experiments, which are close to the nominal 95% level for large n . This is consistent with the results of Corollary 1 and Theorem 4. Figure 2 shows the histograms of $[\widehat{\Theta} - \Theta^* \mathbf{R}_1]_{1,1}$, $[\widehat{\Phi} - \Phi^* \mathbf{R}_2]_{1,1}$ and $[\widehat{\Lambda}_1 - \mathbf{R}_1 \Lambda_1 \mathbf{R}_2]_{1,1}$ after standardization, together with the standard normal density curve, under three types of networks with $n = 1600, T = 100$. It is shown that the empirical distributions are approximated well by Gaussian distributions.

4.2 Real data

The Correlates Of War (COW, Barbieri and Keshk, 2016) is a comprehensive project containing a variety of datasets capturing international behavior over the years. We apply the

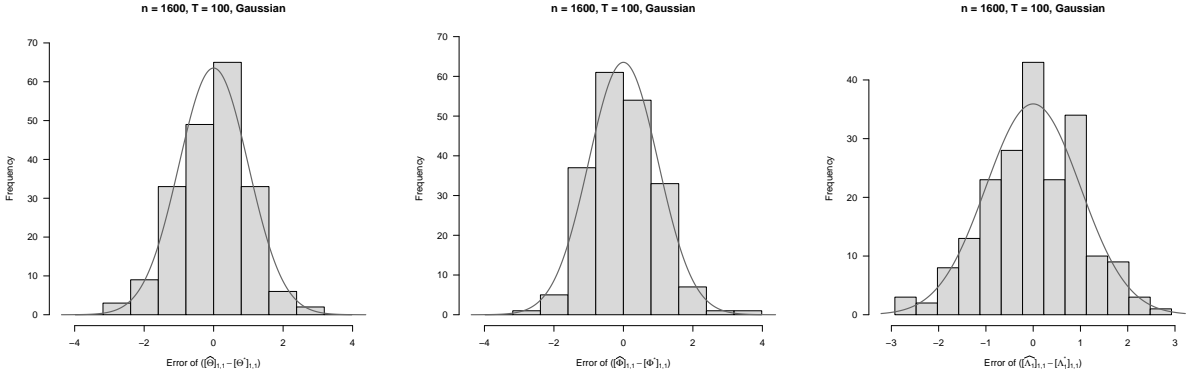


(a) $T = 50$

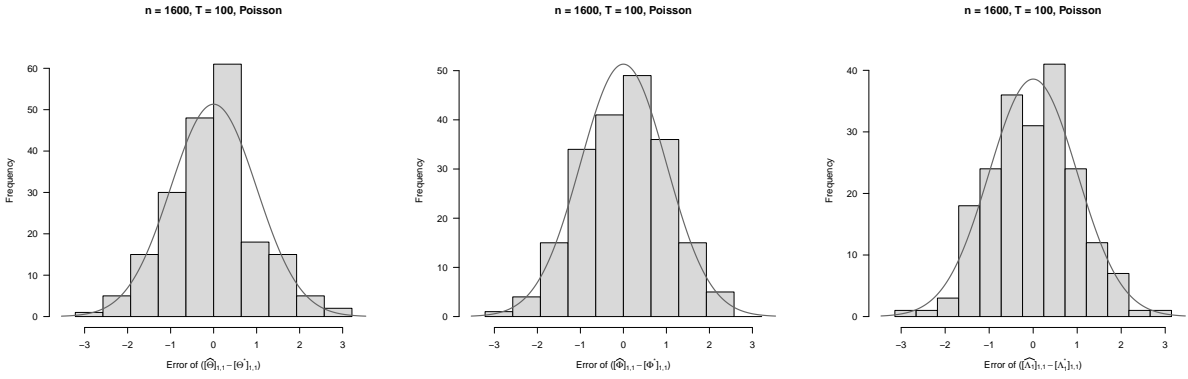


(b) $T = 100$

Figure 1: Boxplots for the estimation errors, $\Delta\Theta$, $\Delta\Phi$, $\Delta\Lambda$, over 200 independent experiments under different settings. Columns correspond to Θ , Φ , and $\{\Lambda_t\}_{t=1}^T$, while rows correspond to Gaussian, Poisson, and Binary settings.



(a) Gaussian



(b) Poisson

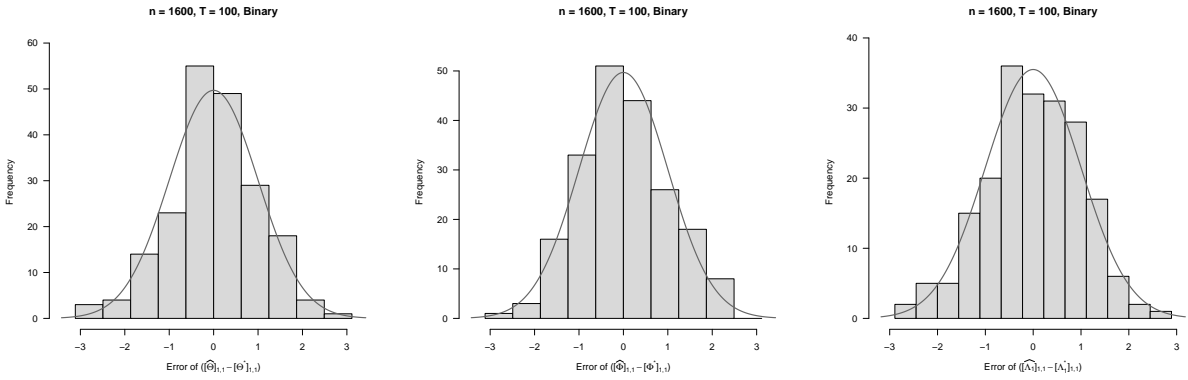


Figure 2: Empirical distributions of $[\hat{\Theta} - \Theta^* \mathbf{R}_1]_{1,1}$, $[\hat{\Phi} - \Phi^* \mathbf{R}_2]_{1,1}$ and $[\hat{\Lambda}_1 - \mathbf{R}_1 \Lambda_1 \mathbf{R}_2]_{1,1}$ after standardization ($n = 1600$, $T = 100$). Gray curves represent the standard normal distribution.

proposed method to analyze the trade dataset from COW, which provides bilateral import value for 207 countries and districts from 1870 to 2014. A subset of 100 active countries is selected from 1965 to 2014 and all import values are transformed by logarithm, while all zero import values are set as a large negative value. This leads to a multilayer network with $n = 100$ nodes and $T = 50$ layers, as well as an adjacency matrix $\mathcal{Y} \in \mathbb{R}^{100 \times 100 \times 50}$ with continuous entries. We apply the Gaussian model such that $\mathcal{Y} = \mathcal{X} + \mathcal{E}$ with each $\mathcal{E}_{i,j,t}$ following Gaussian distribution with mean 0 and unknown variance σ_0^2 .

In order to determine the dimensions of the latent positions, we examine the singular values of the two-sided centered data matrices $\mathbf{J}_n \mathcal{M}_m(\mathcal{Y}) \mathbf{J}_{n,T}^\top, m \in [2]$. The scree plots reveal a clear elbow at both the third singular values, and thus we choose $k_1 = k_2 = 3$. Further, we choose $k_\alpha = k_\beta = 1$.

(a) Top 15 countries				(b) Bottom 15 countries			
Country	Code	Region	$[\widehat{\Theta}]_{:,1}$	Country	Code	Region	$[\widehat{\Theta}]_{:,1}$
United States of America	USA	North America	1.657	Ukraine	UKR	Europe	-1.003
Japan	JPN	Asia-Pacific	1.588	Slovenia	SLV	Europe	-1.015
United Kingdom	UKG	Europe	1.582	Belarus	BLR	Europe	-1.082
France	FRN	Europe	1.565	Estonia	EST	Europe	-1.101
Italy	ITA	Europe	1.556	Lithuania	LIT	Europe	-1.104
Netherlands	NTH	Europe	1.506	Croatia	CRO	Europe	-1.106
Switzerland	SWZ	Europe	1.465	Latvia	LAT	Europe	-1.115
Sweden	SWD	Europe	1.448	Kazakhstan	KZK	Asia-Pacific	-1.216
Belgium	BEL	Europe	1.436	Yemen	YEM	Middle East	-1.219
Spain	SPN	Europe	1.431	Macedonia	MAC	Europe	-1.345
Canada	CAN	North America	1.431	Azerbaijan	AZE	Europe	-1.380
Brazil	BRA	South America	1.425	Moldova	MLD	Europe	-1.418
Austria	AUS	Europe	1.369	Uzbekistan	UZB	Asia-Pacific	-1.494
Denmark	DEN	Europe	1.366	Turkmenistan	TKM	Asia-Pacific	-1.556
Australia	AUL	Asia-Pacific	1.337	Kyrgyzstan	KYR	Asia-Pacific	-1.577

Table 2: Top and bottom 15 countries by $[\widehat{\Theta}]_{:,1}$

The top 15 countries with the highest value of $[\widehat{\Theta}]_{:,1}$, as shown in Table 2, are mostly large, high-income, industrialized economies. Meanwhile, countries with low values are mostly peripheral exporters, that have weaker integration into global trade network. Hence $[\widehat{\Theta}]_{:,1}$ reflects the degree of “global-hubness” of the exporters, it distinguishes core industrialized economies (global hubs) from peripheral, less integrated exporters. As for the second component of $\widehat{\Theta}$, it seems to assign high values on emerging economies. As shown in Table 3, top

15 countries are largely post-Soviet countries, with China and South Korea also appearing as raising economic power over the past decades. At the other end of the spectrum, the country with the lowest score is Yugoslavia, a country that dissolved in the early 1990s. Overall, this component highlights patterns specific to emerging economies. Table 4, together with Figure 3b, reveals a strong pattern of geographical clustering: countries from the same region tend to take on similar value of $[\widehat{\Theta}]_{:,3}$. In Figure 3b, countries in North and South America cluster toward the upper part of the plot, whereas, Middle-Eastern countries gather near the bottom. The three components of $\widehat{\Phi}$ exhibit patterns similar to those of $\widehat{\Theta}$. The first component loads heavily on large, developed economies with strong consumption demand, while the second component assigns high values to emerging markets. We can also observe a degree of geographical cluster on $[\widehat{\Phi}]_{:,3}$. Further details are provided in the supplementary material.

(a) Top 15 countries				(b) Bottom 15 countries			
Country	Code	Region	$[\widehat{\Theta}]_{:,2}$	Country	Code	Region	$[\widehat{\Theta}]_{:,2}$
Germany	GMY	Europe	2.507	Paraguay	PAR	South America	-1.098
Czech Republic	CZR	Europe	2.070	Bahamas	BHM	North America	-1.121
Ukraine	UKR	Europe	1.947	Jamaica	JAM	North America	-1.174
Slovakia	SLO	Europe	1.920	Kuwait	KUW	Middle East	-1.185
Slovenia	SLV	Europe	1.862	Tanzania	TAZ	Africa	-1.213
Croatia	CRO	Europe	1.563	Trinidad and Tobago	TRI	North America	-1.240
Lithuania	LIT	Europe	1.547	Mozambique	MZM	Africa	-1.280
Belarus	BLR	Europe	1.543	Zambia	ZAM	Africa	-1.398
Estonia	EST	Europe	1.529	Angola	ANG	Africa	-1.414
Latvia	LAT	Europe	1.460	Myanmar	MYA	Asia-Pacific	-1.478
Kazakhstan	KZK	Asia-Pacific	1.218	Sudan	SUD	Africa	-1.532
China	CHN	Asia-Pacific	0.914	Libya	LIB	Africa	-1.659
South Korea	ROK	Asia-Pacific	0.796	Liberia	LBR	Africa	-1.935
United States of America	USA	North America	0.766	Iraq	IRQ	Middle East	-2.187
Italy	ITA	Europe	0.759	Yugoslavia	YUG	Europe	-3.682

Table 3: Top and bottom 15 countries by $[\widehat{\Theta}]_{:,2}$

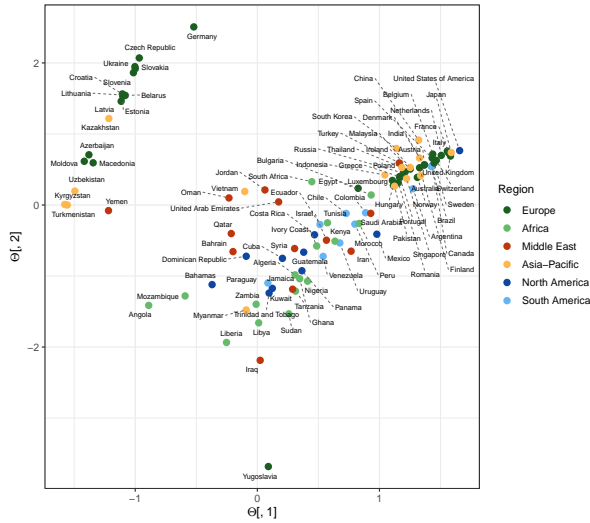
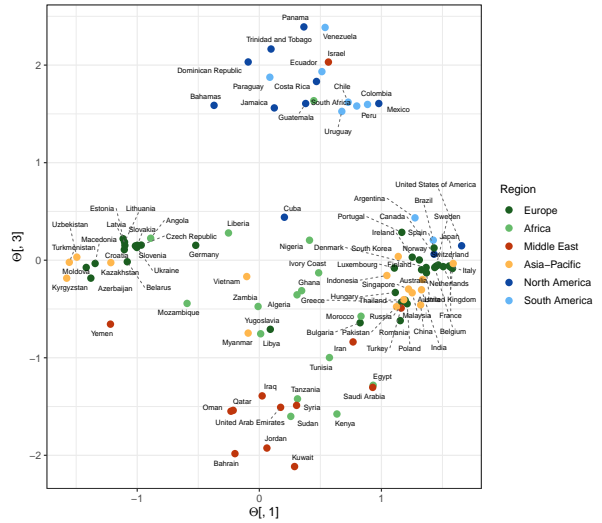
The sequence $\{\mathbf{\Lambda}_t\}_{t=1}^T$ captures the evolution of the connection pattern of the multi-layer network. Specifically, $[\mathbf{\Lambda}_t]_{i,j}$ is the coefficient for the interaction effect between the i -th column of Θ and the j -th column of Φ . Figure 4a and Figure 4c show $\{[\widehat{\Lambda}_t]_{1,1}\}_{t=1}^T$ and $\{[\widehat{\Lambda}_t]_{3,3}\}_{t=1}^T$, respectively. Figure 4a exhibits a marked structural break in the early 1990s, coinciding with the breakup of the Soviet Union. The emergence of new countries

(a) Top 15 countries

Country	Code	Region	$[\hat{\Theta}]_{:,3}$
Panama	PAN	North America	2.392
Venezuela	VEN	South America	2.386
Trinidad and Tobago	TRI	North America	2.165
Dominican Republic	DOM	North America	2.032
Israel	ISR	Middle East	2.031
Ecuador	ECU	South America	1.933
Paraguay	PAR	South America	1.876
Costa Rica	COS	North America	1.832
South Africa	SAF	Africa	1.635
Chile	CHL	South America	1.620
Mexico	MEX	North America	1.606
Guatemala	GUA	North America	1.606
Colombia	COL	South America	1.597
Bahamas	BHM	North America	1.587
Peru	PER	South America	1.581

(b) Bottom 15 countries

Country	Code	Region	$[\hat{\Theta}]_{:,3}$
Iran	IRN	Middle East	-0.838
Tunisia	TUN	Africa	-0.998
Egypt	EGY	Africa	-1.282
Saudi Arabia	SAU	Middle East	-1.304
Iraq	IRQ	Middle East	-1.391
Tanzania	TAZ	Africa	-1.421
Syria	SYR	Middle East	-1.488
United Arab Emirates	UAE	Middle East	-1.508
Qatar	QAT	Middle East	-1.539
Oman	OMA	Middle East	-1.548
Kenya	KEN	Africa	-1.577
Sudan	SUD	Africa	-1.601
Jordan	JOR	Middle East	-1.926
Bahrain	BAH	Middle East	-1.983
Kuwait	KUW	Middle East	-2.115

Table 4: Top and bottom 15 countries by $[\hat{\Theta}]_{:,3}$ (a) $[\hat{\Theta}]_{:,1}$ and $[\hat{\Theta}]_{:,2}$ (b) $[\hat{\Theta}]_{:,1}$ and $[\hat{\Theta}]_{:,3}$ Figure 3: Visualizations of the $\{\hat{\theta}_i\}_{i=1}^n$. Panel (a) shows the first two dimensions and panel (b) shows the first and third dimension. Countries are colored according to region.

and the dissolution of others introduced substantial structural changes to the global trade network. Meanwhile, the trend in Figure 4c suggests a gradual reorientation of the global trade structure, consistent with the rise of East Asia and the deepening of European economic integration. We further test whether the structural changes are significant by the multiple testing procedure described in Section 3.2 with $t' = t - 1$ and $\alpha = 0.05$. To this end, we estimate the noise variance σ_0^2 by the sample variance of the entries in the tensor $[\mathcal{Y}; \mathbf{J}_n, \mathbf{J}_n, \mathbf{I}_T] - [\widehat{\mathcal{S}}; \widehat{\Theta}, \widehat{\Phi}, \mathbf{I}_T]$. Theoretical details are provided in the supplement. The detected change points are $\{1966, 1971, 1975, 1990, 1992, 1993, 1994, 2001\}$. These change points align with major historical shifts in the global economy. The cluster of years in the early 1990s (1990-1994) directly corresponds to the collapse of the Soviet Union and the economic reorientation of Eastern Europe. The change point around 2001 coincides with China’s entry into the WTO, which dramatically reshaped global supply chains. Earlier shifts, like 1971 and 1975, match the end of the post-war monetary system and the oil price shocks, respectively. The year 1966 marks an early transition towards deeper regional integration and trade liberalization. Figure 4b and Figure 4d further show the first order difference sequences $\{[\widehat{\Lambda}_t]_{1,1} - [\widehat{\Lambda}_{t-1}]_{1,1}\}_{t=2}^T$ and $\{[\widehat{\Lambda}_t]_{3,3} - [\widehat{\Lambda}_{t-1}]_{3,3}\}_{t=2}^T$, as well as the original and Bonferroni-corrected 95% confidence intervals at each time points, confirming such structural changes in the early 1990s and around 2001. Figures for the other $\{[\widehat{\Lambda}_t]_{i,j}\}_{t=2}^T$ are deferred to the supplementary material.

5 Conclusions

This paper proposes a new generalized multilayer latent space model to analyze multilayer network data. A novel *unfolding and fusion* algorithm is proposed to estimate the latent positions and connection matrices, which is computationally friendly by avoiding large-scale tensor optimization. Asymptotic results are derived for the proposed estimators, which facili-

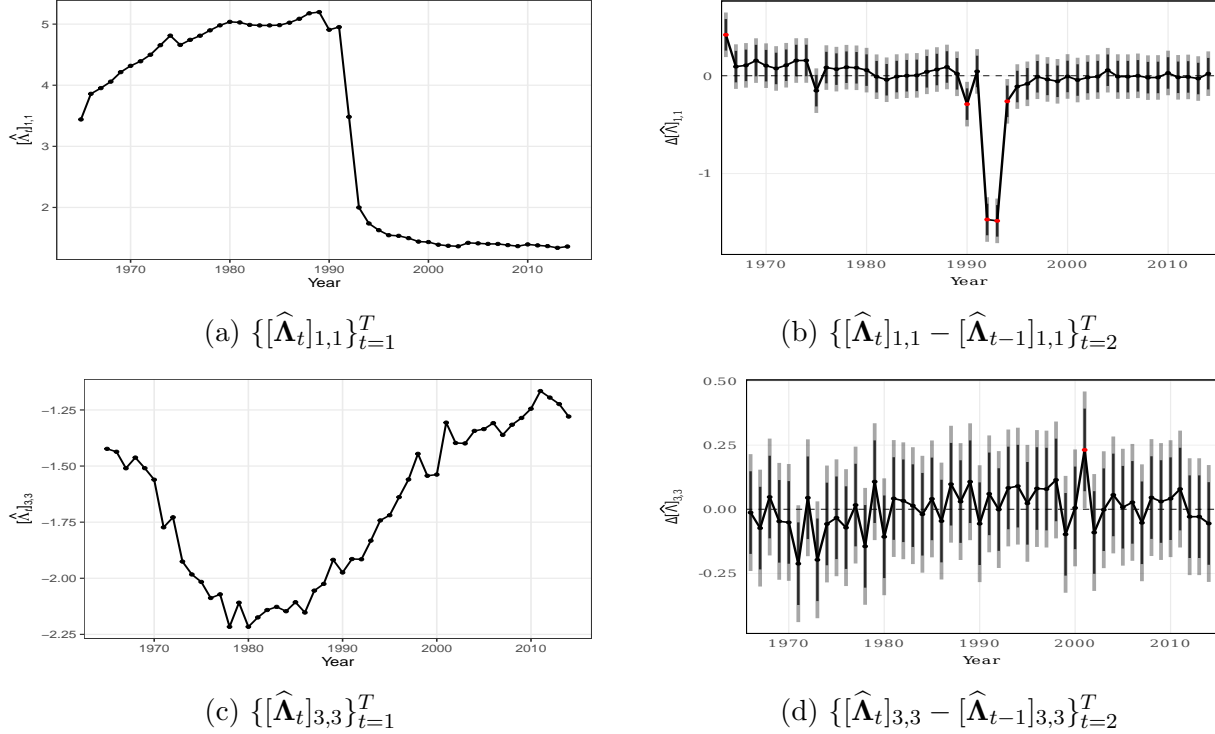


Figure 4: Panels (a)–(b) show the sequence and first-order difference for $[\widehat{\Lambda}_t]_{1,1}$, while panels (c)–(d) display those for $[\widehat{\Lambda}_t]_{3,3}$, with two 95%-confidence intervals at each time point in the difference plots: the black intervals are the original 95%-confidence intervals while the gray intervals are Bonferroni-corrected ones. The red dots indicate statistically significant change points identified using the Bonferroni-corrected confidence intervals.

tate confidence interval construction for the estimated latent positions and testing hypothesis for network structural changes.

One possible future direction is to explore layer sparsity and node degree heterogeneity in the proposed generalized multilayer latent space model, such as the scenario considered in [Ke and Wang \(2025\)](#). Another direction is to investigate the dynamics on the connection matrices for dynamic networks to facilitate network prediction. For example, the matrix autoregressive model ([Chen et al., 2021](#)) could be incorporated into our model setting. In addition, incorporating node-wise or edge-wise covariates into the model framework is also feasible, for example, as in [Xu et al. \(2023\)](#) and [Zhang et al. \(2022\)](#). It would be interesting to test the effect of such covariates on the multilayer network structure. We leave these

topics for future investigation.

References

- A. Alves, L. G., Mangioni, G., Rodrigues, F. A., Panzarasa, P., and Moreno, Y. (2018). Unfolding the complexity of the global value chain: Strength and entropy in the single-layer, multiplex, and multi-layer international trade networks. *Entropy. An International and Interdisciplinary Journal of Entropy and Information Studies*, 20(909).
- Agterberg, J. and Zhang, A. (2024). Statistical inference for low-rank tensors: Heteroskedasticity, subgaussianity, and applications. *arXiv preprint arXiv:2410.06381*.
- Arroyo, J., Athreya, A., Cape, J., Chen, G., Priebe, C. E., and Vogelstein, J. T. (2021). Inference for multiple heterogeneous networks with a common invariant subspace. *Journal of Machine Learning Research*, 22(142):1–49.
- Baggio, J. A., BurnSilver, S. B., Arenas, A., Magdanz, J. S., Kofinas, G. P., and Domenico, M. D. (2016). Multiplex social ecological network analysis reveals how social changes affect community robustness more than resource depletion. *Proceedings of the National Academy of Sciences*, 113(48):13708–13713.
- Bai, J. (2003). Inferential theory for factor models of large dimensions. *Econometrica*, 71:135–171.
- Bai, J. and Li, K. (2012). Statistical analysis of factor models of high dimension. *The Annals of Statistics*, 40:436–465.
- Barbieri, K. and Keshk, O. M. G. (2016). Correlates of war project trade data set codebook, version 4.0. <https://correlatesofwar.org>. Data set covering bilateral and national trade flows between states, 1870–2014.

- Barbillon, P., Donnet, S., Lazega, E., and Bar-Hen, A. (2017). Stochastic block models for multiplex networks: an application to a multilevel network of researchers. *Journal of the Royal Statistical Society Series A: Statistics in Society*, 180(1):295–314.
- Bhattacharyya, S. and Chatterjee, S. (2017). Spectral clustering for multiple sparse networks. *Biometrika*, 103(1):1–28.
- Candes, E. and Recht, B. (2012). Exact matrix completion via convex optimization. *Communications of the ACM*, 55(6):111–119.
- Chen, R., Xiao, H., and Yang, D. (2021). Autoregressive models for matrix-valued time series. *Journal of Econometrics*, 222(1):539–560.
- Chen, Y. and Li, X. (2022). Determining the number of factors in high-dimensional generalized latent factor models. *Biometrika*, 109(3):769–782.
- Chen, Y., Li, X., and Zhang, S. (2020). Structured latent factor analysis for large-scale data: Identifiability, estimability, and their implications. *Journal of the American Statistical Association*, 115:1756–1770.
- D’Angelo, S., Murphy, T. B., and Alfö, M. (2019). Latent space modelling of multidimensional networks with application to the exchange of votes in Eurovision song contest. *The Annals of Applied Statistics*, 13(2).
- Dickison, M. E., Magnani, M., and Rossi, L. (2016). *Multilayer social networks*. Cambridge University Press.
- Fan, J., Liao, Y., and Wang, W. (2016). Projected principal component analysis in factor models. *The Annals of Statistics*, 44(1):219.
- Gollini, I. and Murphy, T. B. (2016). Joint modeling of multiple network views. *Journal of Computational and Graphical Statistics*, 25(1):246–265.

- Han, Q., Xu, K., and Airoldi, E. (2015). Consistent estimation of dynamic and multi-layer block models. In *International Conference on Machine Learning*, pages 1511–1520. PMLR.
- Han, R., Willett, R., and Zhang, A. R. (2022). An optimal statistical and computational framework for generalized tensor estimation. *The Annals of Statistics*, 50:1–29.
- He, Y., Sun, J., Tian, Y., Ying, Z., and Feng, Y. (2025). Semiparametric modeling and analysis for longitudinal network data. *The Annals of Statistics*, 53(4):1406–1430.
- Hoff, P., Raftery, A., and Handcock, M. (2002). Latent space approaches to social network analysis. *Journal of the American Statistical Association*, 97:1090–1098.
- Jing, B.-Y., Li, T., Lyu, Z., and Xia, D. (2021). Community detection on mixture multilayer networks via regularized tensor decomposition. *The Annals of Statistics*, 49(6):3181–3205.
- Ke, Z. T. and Wang, J. (2025). Optimal network membership estimation under severe degree heterogeneity. *Journal of the American Statistical Association*, 120(550):948–962.
- Lei, J., Chen, K., and Lynch, B. (2020). Consistent community detection in multi-layer network data. *Biometrika*, 107(1):61–73.
- Li, J., Xu, G., and Zhu, J. (2023). Statistical inference on latent space models for network data. *arXiv preprint arXiv:2312.06605*.
- Liu, X., Maiorino, E., Halu, A., Glass, K., Prasad, R. B., Loscalzo, J., Gao, J., and Sharma, A. (2020). Robustness and lethality in multilayer biological molecular networks. *Nature Communications*, 11(1):6043.
- MacDonald, P. W., Levina, E., and Zhu, J. (2022). Latent space models for multiplex networks with shared structure. *Biometrika*, 109(3):683–706.

- Núñez-Carpintero, I., Rigau, M., Bosio, M., O'Connor, E., Spendiff, S., Azuma, Y., Topf, A., Thompson, R., 't Hoen, P. A. C., Chamova, T., Tournev, I., Guerguelcheva, V., Laurie, S., Beltran, S., Capella-Gutiérrez, S., Cirillo, D., Lochmüller, H., and Valencia, A. (2024). Rare disease research workflow using multilayer networks elucidates the molecular determinants of severity in Congenital Myasthenic Syndromes. *Nature Communications*, 15(1):1227.
- Paul, S. and Chen, Y. (2016). Consistent community detection in multi-relational data through restricted multi-layer stochastic blockmodel. *Electronic Journal of Statistics*, 10:3807–3870.
- Rabe-Hesketh, S. and Skrondal, A. (2004). *Generalized latent variable modeling: Multilevel, longitudinal, and structural equation models*. Chapman and Hall/CRC, New York, NY.
- Ren, Z.-M., Zeng, A., and Zhang, Y.-C. (2020). Bridging nestedness and economic complexity in multilayer world trade networks. *Humanities and Social Sciences Communications*, 7(1):156.
- Salter-Townshend, M. and McCormick, T. H. (2017). Latent space models for multiview network data. *The Annals of Applied Statistics*, 11(3):1217.
- Su, W., Guo, X., and Yang, Y. (2026). Limit results for estimation of connectivity matrix in multi-layer stochastic block models. *Journal of Statistical Planning and Inference*, 241:106313.
- Wang, F. (2022). Maximum likelihood estimation and inference for high dimensional generalized factor models with application to factor-augmented regressions. *Journal of Econometrics*, 229(1):180–200.
- Wilson, J. D., Palowitch, J., Bhamidi, S., and Nobel, A. B. (2017). Community extraction

- in multilayer networks with heterogeneous community structure. *Journal of Machine Learning Research*, 18(149):1–49.
- Xia, D., Zhang, A. R., and Zhou, Y. (2022). Inference for low-rank tensors—no need to debias. *The Annals of Statistics*, 50(2):1220–1245.
- Xie, F. (2024). Bias-corrected joint spectral embedding for multilayer networks with invariant subspace: Entrywise eigenvector perturbation and inference. *IEEE Trans. Inf. Theor.*, 70(12):9036–9083.
- Xu, S., Zhen, Y., and Wang, J. (2023). Covariate-assisted community detection in multi-layer networks. *Journal of Business & Economic Statistics*, 41(3):915–926.
- Yu, Y., Wang, T., and Samworth, R. J. (2015). A useful variant of the davis–kahan theorem for statisticians. *Biometrika*, 102:315–323.
- Yuan, Y. and Qu, A. (2021). Community detection with dependent connectivity. *The Annals of Statistics*, 49(4):2378–2428.
- Zhang, H., Chen, Y., and Li, X. (2020a). A note on exploratory item factor analysis by singular value decomposition. *Psychometrika*, 85(2):358–372.
- Zhang, H. and Wang, J. (2025). Efficient estimation for longitudinal networks via adaptive merging. *Journal of the American Statistical Association*, 120(551):1683–1694.
- Zhang, X., Xu, G., and Zhu, J. (2022). Joint latent space models for network data with high-dimensional node variables. *Biometrika*, 109(3):707–720.
- Zhang, X., Xue, S., and Zhu, J. (2020b). A flexible latent space model for multilayer networks. In III, H. D. and Singh, A., editors, *Proceedings of the 37th International Conference on Machine Learning*, volume 119 of *Proceedings of Machine Learning Research*, pages 11288–11297. PMLR.